

Molecule Mixture Detection and Design for MC Systems with Non-linear, Cross-reactive Receiver Arrays

Bastian Heinlein, Kaikai Zhu, Sümeyye Carkit-Yilmaz, Sebastian Lotter, Helene M. Loos, Andrea Buettner, Yansha Deng, Robert Schober, and Vahid Jamali

Abstract

Air-based molecular communication (MC) has the potential to be one of the first MC systems to be deployed in real-world applications, enabled by commercially available sensors. However, these sensors usually exhibit non-linear and cross-reactive behavior, contrary to the idealizing assumption of linear and perfectly molecule type-specific sensing often made in the MC literature. To address this mismatch, we propose several detectors and transmission schemes for a molecule mixture communication system where the receiver (RX) employs non-linear, cross-reactive sensors. All proposed schemes are based on the first- and second-order moments of the symbol likelihoods that are fed through the non-linear RX using the Unscented Transform. In particular, we propose an approximate maximum likelihood (AML) symbol-by-symbol detector for inter-symbol interference (ISI)-free transmission scenarios and a complementary mixture alphabet design algorithm which accounts for the RX characteristics. When significant ISI is present at high data rates, the AML detector can be adapted to exploit statistical ISI knowledge. Additionally, we propose a sequence detector which combines information from multiple symbol intervals. For settings where sequence detection is not possible due to extremely limited computational power at the RX, we propose an adaptive transmission scheme which can be combined with symbol-by-symbol detection. Using computer simulations, we validate all proposed detectors and algorithms based on the responses of commercially available sensors as well as artificially generated sensor data incorporating the characteristics of metal-oxide semiconductor sensors. By employing a general system model that accounts for transmitter noise, ISI, and general non-linear, cross-reactive RX arrays, this work enables reliable communication for a large class of MC systems.

Bastian Heinlein, Kaikai Zhu, Sümeyye Carkit-Yilmaz, Sebastian Lotter, Helene M. Loos, Andrea Buettner, and Robert Schober are with Friedrich-Alexander-Universität Erlangen-Nürnberg, Erlangen, Germany. Bastian Heinlein and Vahid Jamali are with Technical University of Darmstadt, Darmstadt, Germany. Yansha Deng is with King's College, London, United Kingdom. Helene M. Loos and Andrea Büttner are also with the Fraunhofer Institute for Process Engineering and Packaging IVV, Freising, Germany. Helene M. Loos is also with Rheinische Friedrich-Wilhelms-Universität Bonn, Bonn, Germany.

This work was funded by the Deutsche Forschungsgemeinschaft (DFG, German Research Foundation) – GRK 2950 – Project-ID 509922606.

This work has been presented in part at the ACM Nanoscale Computing and Communications Conference, 2025, [1].

I. INTRODUCTION

Molecular communication (MC) constitutes a new paradigm in communication engineering by employing molecules for information transmission in scenarios where electro-magnetic (EM) wave-based communication is not practical such as for interfacing with biological entities via chemical signals or in EM wave-denied environments [2]. While most work in MC has considered scenarios where information is encoded into the concentration of a single molecule type, i.e., concentration shift keying (CSK), modulation schemes employing multiple molecules offer additional degrees of freedom. The arguably simplest example of such a multi-molecule scheme is molecule shift keying (MSK) where the type of molecule that is released in a symbol interval indicates the transmitted symbol, promising higher data rates compared to CSK [3]. Based on [3], a variety of more complex modulation schemes employing multiple molecule types have been proposed to further aid inter-symbol interference (ISI) mitigation, deal with time-varying channels, and increase data rate, e.g., [4]–[7].

However, most existing literature on multi-molecule modulation schemes assumes direct access to the concentration c_s of each molecule type $s \in \{1, \dots, S\}$ through a molecule counting receiver whose response r_s to the s -th molecule type is linearly proportional to c_s , i.e., $r_s \sim c_s$. Here, S denotes the total number of considered molecule types. While the concentrations of individual molecule types can in principle be measured in macro-scale applications, e.g., using proton-transfer-reaction mass spectrometry or membrane inlet mass spectrometry, these devices are prohibitively expensive for most applications and are not suitable for mass deployment [8]. On the other hand, cheaper sensors exist, such as optical sensors for liquid-based MC or metal-oxide semiconductor (MOS) sensors for air-based MC, but these sensors are usually cross-reactive or non-linear or both. For example, molecules have often overlapping absorption spectra, rendering optical sensors **cross-reactive** [9], [10], i.e., the sensor response r at a particular wavelength is given by $r = w_1 \cdot c_1 + \dots + w_S \cdot c_S$, where w_s represents the weighting factor for the s -th molecule type. MOS sensors, on the other hand, are well-known to be **non-linear**. Specifically, they exhibit power-law behavior, i.e., $r = a \cdot c^b$, where $a, b \in \mathbb{R}$ [11]. In practice, MOS sensors also react to multiple molecule types at once [12], i.e., they are both non-linear and cross-reactive at the same time. If a sensor is both cross-reactive and non-linear, its response is described by a non-linear function $f(c_1, \dots, c_S)$.

Because experimental work in MC usually relies on such non-linear or cross-reactive sensors, the experimentally implemented modulation schemes have been comparatively simple so

far: While the use of optical sensors for liquid-based multi-molecule communication has been investigated in [9], [10], [13], these testbeds are limited to a small number of molecule types and the molecule alphabets were chosen ad hoc, neglecting opportunity for improved system performance by optimized molecule alphabets. MOS sensors, on the other hand, have been employed mostly for CSK transmissions, also with ad hoc chosen alphabets, e.g., [14], [15]. The work in [16] is a notable exception among the air-borne testbeds employing MOS sensors: Here, information is transmitted by releasing either no molecules, ethanol, acetone, or both and recovered by two MOS sensors at the receiver (RX). However, this work does not investigate higher-order modulation schemes and relies only on an ad hoc chosen alphabet.

We attribute the absence of low-cost practical MC systems employing higher-order multi-molecule modulation schemes and non-linear, cross-reactive RXs in part to a lack of a corresponding theoretical foundation. The primary work to theoretically investigate a macro-scale RX that is both cross-reactive and non-linear is [17]. There, a simple receptor array leveraging compressive sensing for symbol detection, inspired by the olfactory system of insects, is investigated in an ISI-free setting. The information is encoded into the concentration of multiple molecule types at once (i.e., into a **molecule mixture**), with the different mixtures being optimized using a greedy algorithm to elicit different responses of the receptor array. However, to fully leverage the potential of multi-molecule communication for higher data rates, ISI has to be considered. Yet, so far, approaches for ISI-mitigation at the transmitter (TX), e.g., via channel coding or by adaptively choosing the amount of molecules transmitted, have been mostly limited to CSK [18]–[20]. On the other hand, schemes for ISI mitigation at the RX typically assume direct access to molecule concentrations and are thus not applicable in settings with non-linear, cross-reactive sensors [18], [21], [22].

A. *Main Contributions*

Motivated by the lack of study on molecule mixture communication with non-linear, cross reactive RX arrays, especially for ISI channels, we propose methods to enable reliable communication in such scenarios. In particular, our key contributions are summarized as follows.

- We introduce a **comprehensive system model** for molecule mixture communication that accounts for various experimentally identified noise sources (i.e., TX, channel, and RX noise) impairing communication performance and an RX employing a non-linear, cross-reactive sensor array. Unlike the conference version of this paper [1], the model accounts

for ISI, thus making it applicable to settings with shorter symbol intervals, as needed to achieve higher data rates.

- To perform detection for this general system model, we employ the approximate likelihoods of the transmitted mixtures based on the **first- and second-order moments** of the RX’s sensor response. We derive the relevant moments by propagating the uncertainty introduced by the noise sources through the system model leveraging the unscented transform (UT).
- In the **ISI-free case**, we leverage these moments to derive an approximate maximum likelihood (AML) symbol-by-symbol detector and a *static*¹ mixture design algorithm (MDA), which optimizes mixtures so that the sensor outputs at the RX are well-separable.
- Extending [1], we also leverage the derived moments to derive several methods to account for ISI: We adapt the AML detector to **take into account statistical information about the ISI**. This symbol-by-symbol detector in conjunction with the previously mentioned MDA is especially suitable for settings where both RX and TX have extremely limited computational capabilities. We also propose a sequence detector to enable lower symbol error rates (SERs) when more computational power is available at the RX. Finally, we propose an adaptive transmission scheme for settings with a computationally more powerful TX, enabling similar SERs as achieved by the sequence detector while requiring only a symbol-by-symbol detector at the RX.

B. Structure and Notation

The remainder of this paper is structured as follows: Section II introduces the proposed system model. Section III then presents the various moment-based detectors. This is followed by the derivation of the MDA and the adaptive transmission scheme in Section IV. Finally, we evaluate the performance of the proposed schemes in Section V before concluding the paper in Section VI.

Notation: Vectors and matrices are denoted by lowercase and uppercase bold letters, respectively. The i -th entry of vector \mathbf{x} is denoted by $[\mathbf{x}]_i$ and the j -th column of matrix \mathbf{C} as $[\mathbf{C}]_j$. The transpose of matrix \mathbf{C} is denoted by \mathbf{C}^T whereas its determinant is denoted by $\det\{\mathbf{C}\}$. Element-wise multiplication of two vectors \mathbf{x} and \mathbf{y} is shown by $\mathbf{x} \odot \mathbf{y}$. The probability density function (pdf) of a random variable (RV) x conditioned on y is given by $p_{x|y}(x|y)$. The expectation of a RV is denoted by $E\{\cdot\}$ and the covariance matrix of a random vector by $\text{Cov}\{\cdot\}$. \mathbf{I} denotes

¹We refer to this algorithm as *static* because it selects an alphabet of molecule mixtures once before the transmission starts and then uses this alphabet for all symbol intervals.

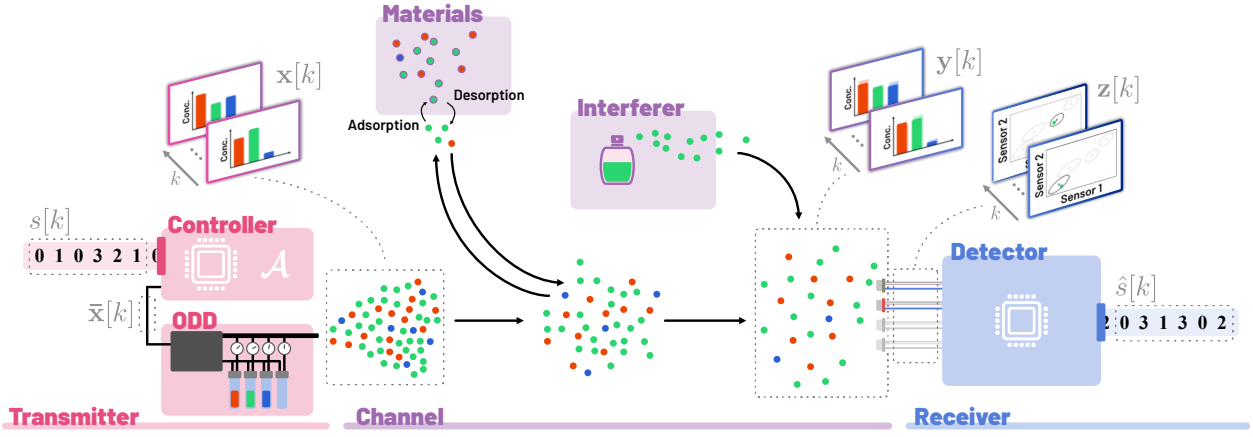


Fig. 1: **System overview.** At the TX, a controller converts a sequence of symbols $s[k]$ to control signals for the odor delivery device (ODD), which should release molecule mixtures $\bar{\mathbf{x}}[k]$, but releases mixtures $\mathbf{x}[k]$ due to hardware imperfections instead. At the RX, molecule mixtures $\mathbf{y}[k]$ are observed because $\mathbf{x}[k]$ is subject to attenuation, e.g., due to dispersion or adsorptions to materials, and interferers might introduce additional molecules. The output of the RX sensor array, $\mathbf{z}[k]$, is then used by the detector to derive a symbol estimate $\hat{s}[k]$.

the identity matrix, $\mathbf{1}$ denotes an all-one column vector, and $\mathbf{0}$, depending on the context, either a column vector or a matrix containing only zeroes. $\|\cdot\|_2$ denotes the ℓ_2 -norm. Sets are shown by calligraphic letters and the cardinality of set \mathcal{A} is denoted by $|\mathcal{A}|$. $\mathcal{U}(\mathcal{A})$ denotes a RV that is uniformly distributed over a set \mathcal{A} . \mathbb{N} and \mathbb{R} denote respectively the sets of real and natural numbers. Analogously, and $\mathbb{R}_{\geq 0}$ and $\mathbb{N}_{\geq 0}$ denote the sets of non-negative real and the non-negative natural numbers, respectively.

II. SYSTEM MODEL

In the following, we first introduce the system model in its general form in Section II-A before characterizing the response of MOS sensors to molecule mixtures and relevant noise distributions in Sections II-B and II-C, respectively.

A. Overview

In this work, we consider the general system model illustrated in Figure 1 that accounts for the three major noise sources reported in the experimental MC literature, namely release noise [14], [15], channel noise [14], and the noise of the sensor array [15], [23]. It also accounts for ISI in the propagation channel and the non-linear, cross-reactive behavior of the sensor array at the RX. To limit complexity, we adopt a single-sample detector, i.e., one sample is taken per symbol interval. Thus, we arrive at the following system model:

$$\mathbf{x}[k] = \bar{\mathbf{x}}[k] + \mathbf{n}^{\text{TX}}(\bar{\mathbf{x}}[k]) \quad (1a)$$

$$\bar{\mathbf{y}}[k] = \sum_{\kappa=0}^{\kappa^{\text{max}}} \mathbf{H}[\kappa] \mathbf{x}[k - \kappa] \quad (1b)$$

$$\mathbf{y}[k] = \bar{\mathbf{y}}[k] + \mathbf{n}^{\text{C}}(\bar{\mathbf{y}}[k]) \quad (1c)$$

$$\mathbf{z}[k] = \mathbf{f}(\mathbf{y}[k]) + \mathbf{n}^{\text{RX}}(\mathbf{f}(\mathbf{y}[k])). \quad (1d)$$

Eq. (1a) describes the noisy release process of the signaling molecules, while (1b) models how the current and previous symbol transmissions accumulate in the propagation channel, and (1c) accounts for the impact of propagation uncertainty and interference. Finally, (1d) describes how the measurements, which are used for symbol detection, relate to the molecule concentrations observed at the RX. The variables appearing in (1a)-(1d) will be explained in the following.

We consider a molecule mixture communication system with mixture alphabet \mathcal{A} of size N . The controller at the TX receives the index $s[k] \in \mathcal{S}_0 = \{1, \dots, N\}$ of the mixture that is to be transmitted in the k -th interval and then determines how many molecules of each type should be released, summarized in $\bar{\mathbf{x}}[k] \in \mathbb{R}_{\geq 0}^S$, where S denotes the number of molecule types available at the TX. The controller then informs the release hardware, such as an odor delivery device (ODD), about the desired release amount $\bar{\mathbf{x}}[k]$ [24]. Eq. (1a) represents that real hardware cannot perfectly control the number of molecules it releases [15], resulting in a **released molecule concentration** $\mathbf{x}[k]$ instead of $\bar{\mathbf{x}}[k]$. We model this release noise by additive noise $\mathbf{n}^{\text{TX}}(\bar{\mathbf{x}}[k])$ which is memory-free but can depend on the desired mixture $\bar{\mathbf{x}}[k]$ and follows the conditional pdf $p_{\mathbf{n}^{\text{TX}}|\bar{\mathbf{x}}[k]}(\mathbf{n}^{\text{TX}})$. It is noted that the number of released molecules cannot be arbitrarily large, but is limited, e.g., by hardware constraints. Therefore, we require that all symbols $\bar{\mathbf{x}}[k] \in \mathcal{A}$ lie in a *feasible set* $\mathcal{F}_{\mathbf{x}} \subseteq \mathbb{R}_{\geq 0}^S$. In this work, we consider $\mathcal{F}_{\mathbf{x}}$ to be a hypercube, i.e., there is an individual constraint on each molecule type. However, our proposed schemes are also applicable to other shapes of the feasible set, e.g., when limiting the total number of released molecules.

Eq. (1b) models the expected molecule concentrations at the RX, $\bar{\mathbf{y}}[k] \in \mathbb{R}_{\geq 0}^S$ after **propagation through the ISI channel**. The fraction of the released molecules expected at the RX is characterized by diagonal channel matrix $\mathbf{H}[k]$. Here, $[\mathbf{H}[k]]_{ii}$ denotes the attenuation factor for molecules of type i released $\kappa \in \{0, \dots, \kappa^{\text{max}}\}$ symbol intervals ago. The specific entries in $\mathbf{H}[k]$ depend, among other things, on the dispersion in the environment, degradation (e.g., due to photochemical oxidation), and adsorption to and desorption from materials in the environment [15], [25], [26]. Here, we assume that the molecules propagate independently from each other.

Eq. (1c) captures how $\bar{\mathbf{y}}[k]$ is affected by **interference or propagation uncertainty** (e.g., each sensor at the RX might observe slightly different molecule concentrations due to the spatial separation of the sensors and diffusion noise), resulting in molecule concentrations $\mathbf{y}[k]$ at the RX. We model the impact of these uncertainties by channel noise $\mathbf{n}^{\text{C}}(\bar{\mathbf{y}}[k])$ which can be signal-

dependent and is distributed according to a conditional pdf $p_{\mathbf{n}^C|\mathbf{y}[k]}(\mathbf{n}^C)$. Throughout this paper, we will use the term sensor input domain (SID) when referring to the moments or observations of the concentrations at the RX.

Finally, (1d) describes how the molecule concentrations $\mathbf{y}[k]$ are converted to the **response of the sensing units**, $\mathbf{z}[k] \in \mathbb{R}^R$, where $[\mathbf{z}[k]]_r$, $r \in \{1, \dots, R\}$, denotes the output of the r -th sensing unit and R is the total number of sensing units at the RX. The detector uses $\mathbf{z}[k]$ to estimate the transmitted symbol as $\hat{s}[k]$. The mapping from $\mathbf{y}[k]$ to $\mathbf{z}[k]$ follows a non-linear function $\mathbf{f}(\cdot)$, whose output depends on multiple molecule concentrations simultaneously. We model the sensing unit as memory-free, which is realistic if the propagation dynamics are slow compared to the sensor dynamics. This is true for various types of practical sensors, including but not limited to optical sensors and many MOS sensors [9], [27], [28]. In practice, the sensing units also introduce measurement noise $\mathbf{n}^{\text{RX}}(\mathbf{f}(\mathbf{y}[k]))$, e.g., thermal noise or quantization noise. For the sake of generality, we again permit signal-dependent measurement noise and characterize it by a conditional pdf $p_{\mathbf{n}^{\text{RX}}|\mathbf{f}(\mathbf{y}[k])}(\mathbf{n}^{\text{RX}})$. Throughout this paper, we will use the term sensor output domain (SOD) when referring to moments or observations related to $\mathbf{z}[k]$.

In summary, we consider a very general system model accounting for the relevant noise sources reported in the experimental MC literature, channel ISI, and a possibly non-linear sensor function.

B. MOS Sensors as a Non-linear, Cross-reactive RX Array

In this work, we consider R MOS sensors as an example of an array of non-linear, cross-reactive sensing units. As already discussed in Section I, it is well established that these sensors exhibit power-law behavior, i.e., their conductance G for a given concentration c of a target gas can be described by $G = a \cdot c^b$, where $a, b \in \mathbb{R}$ are constants specific to the considered combination of sensor and target gas [11]. However, there is no clear consensus on the function that describes the response to gas mixtures. Instead, a variety of models have been proposed in the literature, e.g., [29]–[32]. Here, we focus on the model originally introduced in [29] since it is applicable to mixtures with more than two components and it was shown to provide a good fit to measurement data in [30]. For the r -th sensor, we have [29]

$$[\mathbf{f}(\mathbf{y})]_r = \mathbf{a}_r^T \mathbf{y}_p - \mathbf{y}_p^T \mathbf{A}_r \mathbf{y}_p. \quad (2)$$

Here, \mathbf{y}_p is a $S \times 1$ vector with entries $[\mathbf{y}_p]_s = [\mathbf{y}]_s^{\mathbf{b}_r}$, where $s \in \{1, \dots, S\}$ and \mathbf{b}_r collects the power-law coefficients of the r -th sensor for each gas. The remaining sensor parameters are captured in \mathbf{a}_r and \mathbf{A}_r , where $[\mathbf{a}_r]_i \geq 0 \forall i$ and $[\mathbf{A}_r]_{ij} \geq 0, \forall i > j$, and $[\mathbf{A}_r]_{ij} = 0$ otherwise.

Remark 1. *Our proposed algorithms are applicable to arbitrary functions $\mathbf{f}(\cdot)$ and are not limited to this specific model for MOS sensors or to MOS sensors in the first place. In fact, our algorithms do not even require a closed-form model for the sensor behavior: One could apply our algorithms to preprocessed measurements, making the algorithms relevant even for digital sensors like the BME680 or the DHT22 sensors which have been used in [33], [34].*

C. Relevant Noise Distributions

Next, we specialize the noise distributions for the system model proposed in Section II-A to relevant special cases that are commonly found in MC. Specifically, we consider two scenarios. In the first scenario, all three noise sources are **signal-independent and Gaussian**, permitting a simplified analytical treatment. This scenario will be referred to as signal-independent noise (SIN) in the remainder of this paper. Signal-independent TX noise, characterized by mean $\boldsymbol{\mu}_{\mathbf{n}^{\text{TX}}}^{\text{SIN}}$ and covariance $\mathbf{C}_{\mathbf{n}^{\text{TX}}}^{\text{SIN}}$, might occur, e.g., due to small errors when controlling the flow rates of an ODD [24] or due to small uncontrollable leakage. Signal-independent RX noise, characterized by mean $\boldsymbol{\mu}_{\mathbf{n}^{\text{RX}}}^{\text{SIN}}$ and covariance $\mathbf{C}_{\mathbf{n}^{\text{RX}}}^{\text{SIN}}$, might be due to quantization noise or thermal noise in electronic components [23]. For high molecule concentrations and controlled propagation environments, the observed number of molecules at the RX converges to its expectation (see [35, Sec. 2.2.2.4]). The channel noise, characterized by $\boldsymbol{\mu}_{\mathbf{n}^{\text{C}}}^{\text{SIN}}$ and covariance $\mathbf{C}_{\mathbf{n}^{\text{C}}}^{\text{SIN}}$, may then be used to represent uncertainty about the amount of background molecules in the environment, e.g., due to unknown interference which is independent of the currently transmitted signal. We consider Gaussian noise for simplicity² since it has been shown to be an accurate approximation in air-based MC [8], [14] and since Gaussian RVs are readily parametrized by their mean and covariance. Yet, the proposed detector and mixture alphabet design algorithm are also applicable to other noise distributions, although possibly with some performance degradation since they exploit only mean and covariance.

We consider a second more challenging scenario of **signal-dependent channel noise (SDCN)**, while the TX and RX noise remain signal-independent and Gaussian (i.e., they are described by $\boldsymbol{\mu}_{\mathbf{n}^{\text{TX}}}^{\text{SIN}}$, $\mathbf{C}_{\mathbf{n}^{\text{TX}}}^{\text{SIN}}$, $\boldsymbol{\mu}_{\mathbf{n}^{\text{RX}}}^{\text{SIN}}$, and $\mathbf{C}_{\mathbf{n}^{\text{RX}}}^{\text{SIN}}$ as before). SDCN $\mathbf{n}^{\text{C}}(\mathbf{y}[k])$, which occurs, e.g., in Poisson channels, is commonly assumed in MC [17] and often approximated as

$$\mathbf{n}^{\text{C}}(\mathbf{y}[k]) = \sqrt{\nu^{\text{C}} \mathbf{y}[k]} \odot \bar{\mathbf{n}}, \quad (3)$$

²We note that Gaussian TX and channel noise can in principle lead to negative concentrations, i.e., unphysical behavior. In these cases, we set the values in the simulations manually to zero. These events occur only in rare circumstances for the adopted parameter setting.

where square root $\sqrt{\cdot}$ is applied element-wise and $\bar{\mathbf{n}}$ is normally distributed with zero-mean and covariance matrix \mathbf{I} . We introduce a scaling factor ν^C to control the noise power introduced by the channel, with $\nu^C = 1$ corresponding to the Gaussian approximation of the Poisson channel.

III. MOMENT-BASED DETECTION FOR NON-LINEAR MODELS

In this section, we present the different proposed detectors, which are all based on the first- and second-order moments of the sensor outputs $\mathbf{z}[k]$. To this end, we first introduce the basic idea behind these detectors in Section III-A before presenting the detectors themselves in Section III-B. Then, in Section III-C, we review how first- and second-order moments can be propagated through non-linear functions using the UT and explain how the UT can be employed to estimate the characteristics of signal-dependent noise. Finally, in Section III-D, we derive the moments required by the detectors.

A. Overview

Since the proposed detectors are inspired by maximum likelihood (ML) detection, we briefly review the optimal ML detector for ISI-free channels (i.e., $\kappa^{\max} = 0$) before outlining the concept behind AML detection and how this idea can be extended to ISI channels. For **ML detection**, the likelihoods of all symbols $s[k] \in \mathcal{S}_0$ are exploited to make decisions. In particular, ML detection is performed according to

$$\hat{s}^{\text{ML}}[k] = \arg \max_{s[k] \in \mathcal{S}_0} p_{\mathbf{z}[k]|s[k]}(\mathbf{z}[k]), \quad (4)$$

where $p_{\mathbf{z}[k]|s[k]}(\mathbf{z}[k])$ denotes the pdf of $\mathbf{z}[k]$ in the SOD domain given a transmitted symbol $s[k]$. ML detection not only yields optimal performance in terms of the SER for equiprobable symbols but also does not require inversion of $\mathbf{f}(\cdot)$, which may not be invertible in the first place. Unfortunately, obtaining the likelihoods in the SOD in closed form may not be possible for non-linear, cross-reactive RX arrays.

Thus, we instead propose an approach for **AML detection** based on the approximate first- and second-order moments of $p_{\mathbf{z}[k]|s[k]}(\mathbf{z}[k])$. In this case, the estimated moments $\hat{\boldsymbol{\mu}}_{\mathbf{z}[k]|s[k]}$ and $\hat{\mathbf{C}}_{\mathbf{z}[k]|s[k]}$ are used to parametrize a pdf $\hat{p}_{\mathbf{z}[k]|s[k]}(\mathbf{z})$ approximating $p_{\mathbf{z}[k]|s[k]}(\mathbf{z}[k])$, so that AML detection can be performed according to:

$$\hat{s}^{\text{AML}}[k] = \arg \max_{s[k] \in \mathcal{S}_0} \hat{p}_{\mathbf{z}[k]|s[k]}(\mathbf{z}[k]). \quad (5)$$

We focus on first- and second-order moments because they are easily propagated through linear systems and the UT provides an efficient tool to approximately propagate them through non-linear functions, as we will discuss in detail in Section III-C. For the approximate pdfs,

we use Gaussian distributions, i.e., $\hat{p}_{\mathbf{z}[k]|s[k]}(\mathbf{z}[k]) = \exp[-\frac{1}{2}(\mathbf{z}[k] - \hat{\boldsymbol{\mu}}_{\mathbf{z}[k]|s[k]})^T \hat{\mathbf{C}}_{\mathbf{z}[k]|s[k]}^{-1}(\mathbf{z}[k] - \hat{\boldsymbol{\mu}}_{\mathbf{z}[k]|s[k]})] [(2\pi)^R \det\{\hat{\mathbf{C}}_{\mathbf{z}[k]|s[k]}\}]^{-1/2}$, since these are readily parametrized by first- and second-order moments and fit well to experimental data [8]. The proposed approach based on first- and second-order moments can be straightforwardly extended to scenarios with ISI by either accounting for the *average* ISI contributed by all past symbol sequences or by employing a sequence detector that exploits decisions from previous symbol intervals to cope with ISI.

B. Proposed Detectors

In Sections III-B1-III-B3, we introduce the different detectors considered in this work before comparing them in Section III-B4. Because all detectors leverage approximate moments that are computed using the UT, see Section III-C, we refer to them as UT-based detectors. All proposed detectors require knowledge of the properties of both TX and RX, i.e., $\mathbf{n}^{\text{TX}}(\bar{\mathbf{x}}[k])$, $\mathbf{n}^{\text{RX}}(\mathbf{f}(\mathbf{y}[k]))$, and $\mathbf{f}(\mathbf{y}[k])$. In practice, these can be obtained via *offline* measurements. Additionally, full channel state information is required, i.e., the channel attenuation $\mathbf{H}[\kappa]$ and $\mathbf{n}^{\text{C}}(\bar{\mathbf{y}}[k])$, both of which can be estimated via pilot symbols. However, the task of channel estimation is out of scope of this work and will be addressed in future contributions.

1) *ISI-unaware Detection*: The ISI-unaware detector, first introduced in the conference version of this paper [1], assumes that the channel is ISI-free, i.e., $\kappa^{\text{max}} = 0$, resulting in (5) with $\hat{p}_{\mathbf{z}[k]|s[k]}(\mathbf{z}[k])$ being parametrized by $\hat{\boldsymbol{\mu}}_{\mathbf{z}[k]|s[k]}$ and $\hat{\mathbf{C}}_{\mathbf{z}[k]|s[k]}$, which will be derived in Section III-D.

2) *Low-Complexity Symbol-by-Symbol Detection*: As we will show in Section V-B, the ISI-unaware detector makes systematic errors in the presence of channel ISI. Therefore, we introduce a low complexity (LC) symbol-by-symbol detector which exploits statistical information about the ISI by averaging over all possible transmitted sequences in the channel memory, resulting in the following decision rule for the symbol estimate $\hat{s}^{\text{LC}}[k]$:

$$\hat{s}^{\text{LC}}[k] = \arg \max_{s[k] \in \mathcal{S}_0} \hat{p}_{\mathbf{z}[k]|\mathcal{S}(s[k])}(\mathbf{z}[k]). \quad (6)$$

Here, $\mathcal{S}(s[k])$ denotes all sequences $\mathbf{s}[k] = [s[k - \kappa^{\text{max}}], \dots, s[k]]$ that contain $s[k]$ and the approximate likelihood is parametrized by $\hat{\boldsymbol{\mu}}_{\mathbf{z}[k]|\mathcal{S}(s[k])}$ and $\hat{\mathbf{C}}_{\mathbf{z}[k]|\mathcal{S}(s[k])}$, which will be derived in Section III-D. While the decisions based on (6) have the same complexity as those for the ISI-unaware detector, (5) the mean and covariance are adapted to account for ISI.

3) *Sequence Detection*: Finally, we introduce the sequence detector, summarized in Algorithm 1, which achieves much lower SERs compared to the LC detector by incorporating knowledge from previous intervals. This detector essentially corresponds to the forward pass

Algorithm 1 Sequence Detector

1: **Initialization**2: Initialize state metrics: $\alpha_{\mathbf{s}[0]} = 1/|\mathcal{S}_0|^{\kappa^{\max}}$ 3: **Iteration**4: **for** $k \in \mathbb{N}_{\geq 0}$ **do**5: Compute Likelihoods: $\hat{p}_{\mathbf{z}[k]|\mathbf{s}[k]}(\mathbf{z}[k]), \forall \mathbf{s}[k]$ 6: State metric: $\alpha'_{\mathbf{s}[k]} = \hat{p}_{\mathbf{z}[k]|\mathbf{s}[k]}(\mathbf{z}[k]) \cdot \sum_{\mathbf{s}[k-1] \in \mathcal{P}(\mathbf{s}[k])} \alpha_{\mathbf{s}[k-1]}$ 7: Normalize metric: $\alpha_{\mathbf{s}[k]} = \alpha'_{\mathbf{s}[k]} / \sum_{\mathbf{s}[k]} \alpha'_{\mathbf{s}[k]}$ 8: Symbol metric: $\beta_{\mathbf{s}[k]} = \sum_{\mathbf{s}[k] \in \mathcal{S}(s[k])} \alpha_{\mathbf{s}[k]}$ 9: Estimate: $\hat{s}^{\text{seq}}[k] = \arg \max_{s[k] \in \mathcal{S}_0} \beta_{s[k]}$ 10: **end for**

of the Bahl-Cocke-Jelinek-Raviv (BCJR) algorithm [36]³. In the following, we introduce the individual steps of the proposed sequence detector.

The algorithm considers each sequence $\mathbf{s}[k] = [s[k], \dots, s[k - \kappa^{\max}]]$ as a *state* to which a state metric $\alpha_{\mathbf{s}[k]}$ is assigned. At initialization, all state metrics are set to identical values following line 2 of the algorithm because there is no prior information available about previously transmitted symbols. Then, we compute in each interval first the approximate likelihood $\hat{p}_{\mathbf{z}[k]|\mathbf{s}[k]}(\mathbf{z}[k])$ of each state $\mathbf{s}[k]$ for the current observation $\mathbf{z}[k]$ (line 5), as will be shown in Section III-D.

Then, we combine these likelihoods with the information from the previous interval where we already computed the metrics $\alpha_{\mathbf{s}[k-1]}$ for each state $\mathbf{s}[k-1]$ to get the unnormalized state metrics $\alpha'_{\mathbf{s}[k]}$ for the current interval (line 6) according to

$$\alpha'_{\mathbf{s}[k]} = \hat{p}_{\mathbf{z}[k]|\mathbf{s}[k]}(\mathbf{z}[k]) \cdot \sum_{\mathbf{s}[k-1] \in \mathcal{P}(\mathbf{s}[k])} \alpha_{\mathbf{s}[k-1]}, \quad (7)$$

where $\mathcal{P}(\mathbf{s}[k])$ denotes the set of all possible sequences $\mathbf{s}[k-1]$ that can precede sequence $\mathbf{s}[k]$.

The metrics $\alpha'_{\mathbf{s}[k]}$ are then normalized to obtain $\alpha_{\mathbf{s}[k]}$ according to

$$\alpha_{\mathbf{s}[k]} = \alpha'_{\mathbf{s}[k]} / \sum_{\mathbf{s}'[k] \in \mathcal{S}} \alpha'_{\mathbf{s}'[k]}, \quad (8)$$

where \mathcal{S} denotes the set of all possible sequences $[s[k], \dots, s[k - \kappa^{\max}]]$. With the new state metrics in place, we can compute the symbol metrics $\beta_{s[k]}$ by marginalizing over the normalized state metrics (line 8). Then, we estimate the symbol as $\hat{s}^{\text{seq}}[k]$ by selecting the symbol with the highest symbol metric (line 9).

³While additional performance gains can be achieved by implementing the full BCJR algorithm (i.e., including the backward pass), this would make symbol decisions available only after the whole sequence has been decoded. Since this would dramatically increase memory requirements, we limit ourselves to the forward pass.

4) *Comparison:* After introducing the different detectors, we now provide a high-level comparison of their relative performance in terms of their **error rates** for a given signal-to-noise ratio (SNR) and computational complexity. In the ISI-free case, all proposed detectors collapse to the ISI-unaware detector resulting in identical SER performance. However, in settings with ISI, the ISI-unaware detector makes systematic decision errors as the ISI shifts the signal means, resulting in a mismatch between its decision regions and the actual sensor outputs, and consequently a high SER independent of the SNR. While the LC alleviates this and achieves a lower SER for sufficient SNRs, the sequence detector achieves the lowest SER among all proposed detectors for a given SNR. In terms of **computational complexity**, the ISI-unaware and the LC detector are identical and require only one likelihood computation per symbol $s[k] \in \mathcal{S}_0$, i.e., their complexity scales linearly with $|\mathcal{S}_0|$. On the other hand, the sequence detector requires one likelihood computation per sequence $\mathbf{s}[k] \in \mathcal{S}$, with $|\mathcal{S}| = |\mathcal{S}_0|^{n_{\max}}$. Additionally, the sequence detector has to store $|\mathcal{S}|$ states and $|\mathcal{S}|$ likelihoods, resulting in a larger memory footprint compared to the ISI-unaware and LC detectors that need to store only $|\mathcal{S}_0|$ states. If the RX is computationally constrained but computational power is available at the TX, the LC detector can be combined with an adaptive transmission scheme, which we will introduce in Section IV-B, to achieve similar SERs like the sequence detector.

C. Exploiting the Unscented Transform

Before deriving the moments for the proposed detectors in Section III-D, we briefly introduce the UT [37] and explain how to leverage it to **propagate moments through non-linear functions** and to estimate moments of complex noise distributions. The UT is used to estimate the mean and covariance of an R -dimensional random vector \mathbf{z} which is obtained by feeding an S -dimensional random vector \mathbf{y} with known mean and covariance through a non-linear function $\mathbf{f}(\cdot)$, i.e., $\mathbf{z} = \mathbf{f}(\mathbf{y})$. The main idea behind the UT, as originally introduced for state estimation [37], is relatively simple: One chooses n_{σ} carefully selected points $\mathbf{y}_{\sigma,i}$, $i = 1, \dots, n_{\sigma}$, so-called sigma points, which match the mean $\boldsymbol{\mu}_{\mathbf{y}}$ and covariance $\mathbf{C}_{\mathbf{y}}$ of \mathbf{y} . These points $\mathbf{y}_{\sigma,i}$ are fed through $\mathbf{f}(\cdot)$ to obtain $\mathbf{f}(\mathbf{y}_{\sigma,i})$. Then, the mean $\boldsymbol{\mu}_{\mathbf{z}}$ and covariance $\mathbf{C}_{\mathbf{z}}$ of \mathbf{z} are estimated as

$$\hat{\boldsymbol{\mu}}_{\mathbf{z}} = \text{E}_{\text{UT}} \{\mathbf{z} | \boldsymbol{\mu}_{\mathbf{y}}, \mathbf{C}_{\mathbf{y}}\} = \frac{1}{n_{\sigma}} \sum_{i=1}^{n_{\sigma}} \mathbf{f}(\mathbf{y}_{\sigma,i}) \quad (9a)$$

$$\hat{\mathbf{C}}_{\mathbf{z}} = \text{COV}_{\text{UT}} \{\mathbf{z} | \boldsymbol{\mu}_{\mathbf{y}}, \mathbf{C}_{\mathbf{y}}\} = \frac{1}{n_{\sigma}} \sum_{i=1}^{n_{\sigma}} (\mathbf{f}(\mathbf{y}_{\sigma,i}) - \hat{\boldsymbol{\mu}}_{\mathbf{z}}) (\mathbf{f}(\mathbf{y}_{\sigma,i}) - \hat{\boldsymbol{\mu}}_{\mathbf{z}})^{\text{T}}. \quad (9b)$$

Here, $E_{\text{UT}}\{\cdot|\cdot\}$ and $\text{Cov}_{\text{UT}}\{\cdot|\cdot\}$ are the operators for the UT-based estimate of the mean and covariance of \mathbf{z} , respectively. We follow the approach in [37] and select $n_\sigma = 2S$ sigma points as $\mathbf{y}_{\sigma,j} = \boldsymbol{\mu}_y + [(SC_y)^{1/2}]_j$ and $\mathbf{y}_{\sigma,j+S} = \boldsymbol{\mu}_y - [(SC_y)^{1/2}]_j$, where $j = 1, \dots, S$, and $(SC_y)^{1/2}$ is obtained using the Cholesky decomposition of SC_y . Note that this is conceptually similar to the idea behind particle filtering, but the UT employs only a few carefully selected points [37].

Remark 2. Besides using the UT to propagate moments through $\mathbf{f}(\cdot)$, we also can use it to estimate the moments of noise $\mathbf{n}(\mathbf{x})$ if the signal \mathbf{x} is described by its mean $\boldsymbol{\mu}_x$ and covariance \mathbf{C}_x and we can write $\mathbf{n}(\mathbf{x})$ as $\mathbf{n}(\mathbf{x}) = \mathbf{g}(\mathbf{x}, \bar{\mathbf{n}})$. Here, $\mathbf{g}(\cdot)$ is a multi-dimensional, possibly non-linear function, and $\bar{\mathbf{n}}$ is an appropriately sized vector of zero-mean, unit-variance identically and independently distributed Gaussian RVs. Then, we can collect \mathbf{x} and $\bar{\mathbf{n}}$ in a vector $\mathbf{x}' = [\mathbf{x}, \bar{\mathbf{n}}]^\text{T}$ with mean $[\boldsymbol{\mu}_x, \mathbf{0}]^\text{T}$ and covariance matrix $[\mathbf{C}_x, \mathbf{0}; \mathbf{0}, \mathbf{I}]$ and apply the UT to $\mathbf{g}(\cdot, \cdot)$ as described before. Formally, we write the UT for mean and covariance estimation of $\mathbf{n}(\mathbf{x})$ for a given $\boldsymbol{\mu}_x$ and \mathbf{C}_x as $E_{\text{UT}}\{\mathbf{n}|\boldsymbol{\mu}_x, \mathbf{C}_x\}$ and $\text{Cov}_{\text{UT}}\{\mathbf{n}|\boldsymbol{\mu}_x, \mathbf{C}_x\}$, respectively.

D. Derivation of the Moments

Next, we show how to propagate the first- and second-order moments through the system model before summarizing how the individual propagation steps can be combined to obtain the final moments required by the proposed detectors. We start by deriving the moments of $\mathbf{x}[k]$ for a given symbol $s[k]$.

Proposition 1 (Moments of \mathbf{x}). *The first- and second-order moments of $\mathbf{x}[k]$ for a memory-free TX can be expressed as:*

$$\boldsymbol{\mu}_{\mathbf{x}[k]|s[k]} = \bar{\mathbf{x}}[k] + \int \mathbf{n}^{\text{TX}} \cdot p_{\mathbf{n}^{\text{TX}}|\bar{\mathbf{x}}[k]}(\mathbf{n}^{\text{TX}}) d\mathbf{n}^{\text{TX}} \quad (10a)$$

$$\mathbf{C}_{\mathbf{x}[k]|s[k]} = \int \mathbf{c}(\mathbf{n}^{\text{TX}}, \boldsymbol{\mu}_{\mathbf{n}^{\text{TX}}|\bar{\mathbf{x}}[k]}) p_{\mathbf{n}^{\text{TX}}|\bar{\mathbf{x}}[k]}(\mathbf{n}^{\text{TX}}) d\mathbf{n}^{\text{TX}}, \quad (10b)$$

where $\mathbf{c}(\boldsymbol{\alpha}, \boldsymbol{\beta}) = (\boldsymbol{\alpha} - \boldsymbol{\beta})(\boldsymbol{\alpha} - \boldsymbol{\beta})^\text{T}$ with random vector $\boldsymbol{\alpha}$ and vector $\boldsymbol{\beta}$, $p_{\mathbf{n}^{\text{TX}}|\bar{\mathbf{x}}[k]}(\mathbf{n}^{\text{TX}})$ is the pdf of $\mathbf{n}^{\text{TX}}(\bar{\mathbf{x}})$, and $\boldsymbol{\mu}_{\mathbf{n}^{\text{TX}}|\bar{\mathbf{x}}[k]}$ is the conditional mean of \mathbf{n}^{TX} for a given $\bar{\mathbf{x}}$.

Proof for (10a). We first apply the expectation operator to (1a) and exploit that the mapping $s[k] \rightarrow \bar{\mathbf{x}}[k]$ is deterministic, yielding

$$\boldsymbol{\mu}_{\mathbf{x}[k]|s[k]} = \bar{\mathbf{x}}[k] + E\{\mathbf{n}^{\text{TX}}(\bar{\mathbf{x}}[k])|\bar{\mathbf{x}}[k]\}.$$

Then, we apply the definition of the first-order moment ($E\{x\} = \int x \cdot p_x(x) dx$ for RV x) to arrive at (10a). \square

Proof for (10b). The proof is analogous to the proof for (10a), only that the definition of the covariance is inserted into the following expression:

$$\mathbf{C}_{\mathbf{x}[k]|s[k]} = \text{Cov}\{\bar{\mathbf{x}}[k] + \mathbf{n}^{\text{TX}}(\bar{\mathbf{x}}[k])|s[k]\} = \underbrace{\text{Cov}\{\bar{\mathbf{x}}[k]|s[k]\}}_{=0} + \text{Cov}\{\mathbf{n}^{\text{TX}}(\bar{\mathbf{x}}[k])|s[k]\}. \quad \square$$

Corollary 1.1 (SIN, SDCN). *For both SIN and SDCN, the TX noise is signal-independent and thus, we have*

$$\boldsymbol{\mu}_{\mathbf{x}[k]|s[k]} = \bar{\mathbf{x}}[k] + \boldsymbol{\mu}_{\mathbf{n}^{\text{TX}}}^{\text{SIN}} \quad (11a)$$

$$\mathbf{C}_{\mathbf{x}[k]|s[k]} = \mathbf{C}_{\mathbf{n}^{\text{TX}}}^{\text{SIN}}. \quad (11b)$$

Proof. Apply $\mathbb{E}\{\cdot\}$ and $\text{Cov}\{\cdot\}$ to (1a) and then exploit that the symbol-independent TX noise is parametrized by $\boldsymbol{\mu}_{\mathbf{n}^{\text{TX}}}^{\text{SIN}}$ and $\mathbf{C}_{\mathbf{n}^{\text{TX}}}^{\text{SIN}}$. \square

Proposition 2 (Moments of $\bar{\mathbf{y}}$ for a given sequence). *The mean and covariance of $\bar{\mathbf{y}}[k]$ for a given symbol sequence $\mathbf{s}[k]$ can be written in terms of the TX noise as follows:*

$$\boldsymbol{\mu}_{\bar{\mathbf{y}}[k]|s[k]} = \sum_{\kappa=0}^{\kappa^{\max}} \mathbf{H}[\kappa] \boldsymbol{\mu}_{\mathbf{x}[k-\kappa]|s[k-\kappa]} \quad (12a)$$

$$\mathbf{C}_{\bar{\mathbf{y}}[k]|s[k]} = \sum_{\kappa=0}^{\kappa^{\max}} \mathbf{H}[\kappa] \mathbf{C}_{\mathbf{x}[k-\kappa]|s[k-\kappa]} \mathbf{H}^{\text{T}}[\kappa]. \quad (12b)$$

Proof for (12a). We exploit the linearity of the expectation operator together with the memory-free property of the TX, i.e., that $\mathbf{x}[k]$ depends only on $s[k]$ and not on previous symbols:

$$\begin{aligned} \boldsymbol{\mu}_{\bar{\mathbf{y}}[k]|s[k]} &= \mathbb{E} \left\{ \sum_{\kappa=0}^{\kappa^{\max}} \mathbf{H}[\kappa] \mathbf{x}[k-\kappa] | s[k] \right\} \\ &= \sum_{\kappa=0}^{\kappa^{\max}} \mathbf{H}[\kappa] \mathbb{E} \{ \mathbf{x}[k-\kappa] | s[k-\kappa] \} = \sum_{\kappa=0}^{\kappa^{\max}} \mathbf{H}[\kappa] \boldsymbol{\mu}_{\mathbf{x}[k-\kappa]|s[k-\kappa]}. \end{aligned} \quad \square$$

Proof for (12b). Analogously, we exploit the memory-free property of the TX, that the covariance operator is linear with regard to sums, and that $\text{Cov}\{\mathbf{W}\mathbf{x}\} = \mathbf{W}\text{Cov}\{\mathbf{x}\}\mathbf{W}^{\text{T}}$:

$$\begin{aligned} \mathbf{C}_{\bar{\mathbf{y}}[k]|s[k]} &= \text{Cov} \left\{ \sum_{\kappa=0}^{\kappa^{\max}} \mathbf{H}[\kappa] \mathbf{x}[k-\kappa] | s[k] \right\} \\ &= \sum_{\kappa=0}^{\kappa^{\max}} \mathbf{H}[\kappa] \text{Cov} \{ \mathbf{x}[k-\kappa] | s[k-\kappa] \} \mathbf{H}^{\text{T}}[\kappa] = \sum_{\kappa=0}^{\kappa^{\max}} \mathbf{H}[\kappa] \mathbf{C}_{\mathbf{x}[k-\kappa]|s[k-\kappa]} \mathbf{H}^{\text{T}}[\kappa]. \end{aligned} \quad \square$$

Corollary 2.1 (SIN, SDCN). *For SIN and SDCN, the mean of $\bar{\mathbf{y}}[k]$ can be decomposed into a symbol-dependent contribution and a constant noise contribution while the covariance is entirely symbol-independent:*

$$\boldsymbol{\mu}_{\bar{\mathbf{y}}[k]|s[k]}^{\text{SIN}} = \underbrace{\sum_{\kappa=0}^{\kappa^{\max}} \mathbf{H}[\kappa] \bar{\mathbf{x}}[k-\kappa]}_{\text{desired}} + \underbrace{\sum_{\kappa=0}^{\kappa^{\max}} \mathbf{H}[\kappa] \boldsymbol{\mu}_{\mathbf{n}^{\text{TX}}}^{\text{SIN}}}_{\text{const. noise}} \quad (13a)$$

$$\mathbf{C}_{\bar{\mathbf{y}}[k]|s[k]}^{\text{SIN}} = \sum_{\kappa=0}^{\kappa^{\max}} \mathbf{H}[\kappa] \mathbf{C}_{\mathbf{n}^{\text{TX}}}^{\text{SIN}} \mathbf{H}^{\text{T}}[\kappa]. \quad (13b)$$

Proof. For the mean decomposition, insert $\boldsymbol{\mu}_{\mathbf{x}[k]|s[k]} = \bar{\mathbf{x}}[k] + \boldsymbol{\mu}_{\mathbf{n}^{\text{TX}}}^{\text{SIN}}$ into (12a). For the covariance, insert $\mathbf{C}_{\mathbf{x}[k]|s[k]} = \mathbf{C}_{\mathbf{n}^{\text{TX}}}^{\text{SIN}}$ into (12b). \square

$$\boldsymbol{\mu}_{\bar{y}[k]|\mathcal{S}(s[k])} = \mathbf{H}[0]\boldsymbol{\mu}_{\mathbf{x}[k]|s[k]} + \sum_{\kappa=1}^{\kappa^{\max}} \mathbf{H}[\kappa] \left(\frac{1}{|\mathcal{S}_0|} \sum_{s \in \mathcal{S}_0} \boldsymbol{\mu}_{\mathbf{x}[k-\kappa]|s} \right) \quad (14a)$$

$$\mathbf{C}_{\bar{y}[k]|\mathcal{S}(s[k])} = \mathbf{H}[0]\mathbf{C}_{\mathbf{x}[k]|s[k]}\mathbf{H}^T[0] + \sum_{\kappa=1}^{\kappa^{\max}} \mathbf{H}[\kappa] \left(\frac{1}{|\mathcal{S}_0|} \sum_{s \in \mathcal{S}_0} (\boldsymbol{\mu}_{\mathbf{x}|s} - \boldsymbol{\mu}')(\boldsymbol{\mu}_{\mathbf{x}|s} - \boldsymbol{\mu}')^T + \mathbf{C}_{\mathbf{x}|s} \right) \mathbf{H}^T[\kappa] \quad (14b)$$

Proposition 3 (Moments of \bar{y} for all possible sequences). *The mean and covariance of $\bar{y}[k]$ for symbol $s[k]$ and unknown previous symbols are described by (14a) and (14b), shown at the top of this page, where $\mathcal{S}(s[k])$ is the set of all sequences $s[k]$ that contain symbol $s[k]$ and we have $\boldsymbol{\mu}' = \frac{1}{|\mathcal{S}_0|} \sum_{s \in \mathcal{S}_0} \boldsymbol{\mu}_{\mathbf{x}|s}$.*

Proof for (14a). Applying the expectation operator to (1b) and exploiting its linearity yields

$$\boldsymbol{\mu}_{\bar{y}[k]|\mathcal{S}(s[k])} = \sum_{\kappa=0}^{\kappa^{\max}} \mathbf{H}[\kappa] \mathbb{E} \{ \mathbf{x}[k - \kappa] | \mathcal{S}(s[k]) \}.$$

Then, we split the sum into two parts, one for $\kappa = 0$ and one for $\kappa > 0$, and exploit that $\mathbb{E} \{ \cdot | \mathcal{S}(s[k]) \} = \mathbb{E} \{ \cdot | s[k] \}$ for $\kappa = 0$ and $\mathbb{E} \{ \cdot | \mathcal{S}(s[k]) \} = \mathbb{E} \{ \cdot | \mathcal{S}_0 \}$ for $\kappa > 0$. This yields

$$\boldsymbol{\mu}_{\bar{y}[k]|\mathcal{S}(s[k])} = \mathbf{H}[0] \mathbb{E} \{ \mathbf{x}[k] | s[k] \} + \sum_{\kappa=1}^{\kappa^{\max}} \mathbf{H}[\kappa] \mathbb{E} \{ \mathbf{x}[k - \kappa] | \mathcal{S}_0 \}.$$

To get the final result, we use $\mathbb{E} \{ \mathbf{x}[k - \kappa] | \mathcal{S}_0 \} = \frac{1}{|\mathcal{S}_0|} \sum_{s \in \mathcal{S}_0} \boldsymbol{\mu}_{\mathbf{x}|s}$ for $\kappa > 0$, where $\boldsymbol{\mu}_{\mathbf{x}|s}$ is the mean of \mathbf{x} for a given symbol s . \square

Proof for (14b). To obtain $\mathbf{C}_{\bar{y}[k]|\mathcal{S}(s[k])}$, we first exploit the linearity of the covariance operator with regard to sums and split the sum into one part for $\kappa = 0$ and one for $\kappa > 0$, yielding

$$\begin{aligned} \mathbf{C}_{\bar{y}[k]|\mathcal{S}(s[k])} &= \mathbf{H}[0] \text{Cov} \{ \mathbf{x}[k] | s[k] \} \mathbf{H}^T[0] \\ &\quad + \sum_{\kappa=1}^{\kappa^{\max}} \mathbf{H}[\kappa] \text{Cov} \{ \mathbf{x}[k - \kappa] | \mathcal{S}_0 \} \mathbf{H}^T[\kappa]. \end{aligned}$$

Then, we can set $\text{Cov} \{ \mathbf{x}[k] | s[k] \} = \mathbf{C}_{\mathbf{x}[k]|s[k]}$ and exploit the law of total covariance for $\kappa > 0$, i.e.,

$$\text{Cov} \{ \mathbf{x}[k - \kappa] | \mathcal{S}_0 \} = \text{Cov} \{ \mathbb{E} \{ \mathbf{x} | s \} | \mathcal{S}_0 \} + \mathbb{E} \{ \text{Cov} \{ \mathbf{x} | s \} | \mathcal{S}_0 \},$$

where we dropped the time index for brevity. We know that $\mathbb{E} \{ \mathbf{x} | s \} = \boldsymbol{\mu}_{\mathbf{x}|s}$ and thus $\text{Cov} \{ \boldsymbol{\mu}_{\mathbf{x}|s} | \mathcal{S}_0 \} = \frac{1}{|\mathcal{S}_0|} \sum_s (\boldsymbol{\mu}_{\mathbf{x}|s} - \boldsymbol{\mu}')(\boldsymbol{\mu}_{\mathbf{x}|s} - \boldsymbol{\mu}')^T$, where $\boldsymbol{\mu}' = \frac{1}{|\mathcal{S}_0|} \sum_{s \in \mathcal{S}_0} \boldsymbol{\mu}_{\mathbf{x}|s}$. Finally, we use that $\mathbb{E} \{ \text{Cov} \{ \mathbf{x} | s \} | \mathcal{S}_0 \} = \frac{1}{|\mathcal{S}_0|} \sum_{s \in \mathcal{S}_0} \mathbf{C}_{\mathbf{x}|s}$ to obtain (14b). \square

Corollary 3.1 (SIN, SDCN). *For both SIN and SDCN, the mean can be divided into a contribution from the current symbol and a constant contribution from noise and the previous symbols.*

The covariance can be divided into one component due to the transmitter noise and into one component due to the lack of knowledge about previously transmitted symbols:

$$\boldsymbol{\mu}_{\bar{\mathbf{y}}[k]|S(s[k])}^{\text{SIN}} = \underbrace{\mathbf{H}[0]\bar{\mathbf{x}}}_{\text{symbol contr.}} + \underbrace{\sum_{\kappa=1}^{\kappa^{\max}} \mathbf{H}[\kappa]\bar{\boldsymbol{\mu}} + \sum_{\kappa=0}^{\kappa^{\max}} \mathbf{H}[\kappa]\boldsymbol{\mu}_{\mathbf{n}^{\text{TX}}}^{\text{SIN}}}_{\text{constant contr.}} \quad (15a)$$

$$\mathbf{C}_{\bar{\mathbf{y}}[k]|S(s[k])}^{\text{SIN}} = \underbrace{\mathbf{C}_{\bar{\mathbf{y}}[k]|s[k]}^{\text{SIN}}}_{\text{TX noise}} + \underbrace{\sum_{\kappa=1}^{\kappa^{\max}} \mathbf{H}[\kappa] \left(\frac{1}{|\mathcal{S}_0|} \sum_{\bar{\mathbf{x}} \in \mathcal{A}} (\bar{\mathbf{x}} - \bar{\boldsymbol{\mu}})(\bar{\mathbf{x}} - \bar{\boldsymbol{\mu}})^{\text{T}} \right) \mathbf{H}^{\text{T}}[\kappa]}_{\text{symbol uncertainty}}, \quad (15b)$$

where $\bar{\boldsymbol{\mu}} = \frac{1}{|\mathcal{S}_0|} \sum_{\bar{\mathbf{x}} \in \mathcal{A}} \bar{\mathbf{x}}$.

Proof for (15a). We insert $\boldsymbol{\mu}_{\mathbf{x}[k]|s[k]} = \bar{\mathbf{x}}[k] + \boldsymbol{\mu}_{\mathbf{n}^{\text{TX}}}^{\text{SIN}}$ into (14a), exploit that $\frac{1}{|\mathcal{S}_0|} \sum_{s[k] \in \mathcal{S}_0} \boldsymbol{\mu}_{\mathbf{x}[k]|s[k]} = \bar{\boldsymbol{\mu}} + \boldsymbol{\mu}_{\mathbf{n}^{\text{TX}}}^{\text{SIN}}$, and split the sums. \square

Proof for (15b). The covariance can be obtained from (14b) by setting $\mathbf{C}_{\mathbf{x}|s} = \mathbf{C}_{\mathbf{n}^{\text{TX}}}^{\text{SIN}}$ and taking the sum over all covariance matrices. For the final expression, we use $\boldsymbol{\mu}_{\mathbf{x}|s} - \boldsymbol{\mu}' = \bar{\mathbf{x}} - \bar{\boldsymbol{\mu}}$. \square

Remark 3. From Corollary 3.1, it can be seen that i) the uncertainty in this setting is strictly larger than that for a specific sequence $\mathbf{s}[k]$ and ii) the symbol uncertainty is the dominating factor in settings with strong ISI. The latter becomes apparent when considering that the mixtures are usually spread over the whole feasible set $\mathcal{F}_{\mathbf{x}}$, so that the covariance $\sum_{\bar{\mathbf{x}} \in \mathcal{A}} (\bar{\mathbf{x}} - \bar{\boldsymbol{\mu}})(\bar{\mathbf{x}} - \bar{\boldsymbol{\mu}})^{\text{T}}$ is comparable to the size of $\mathcal{F}_{\mathbf{x}}$, whereas $\mathbf{C}_{\mathbf{n}^{\text{TX}}}^{\text{SIN}}$ is typically much smaller than $\mathcal{F}_{\mathbf{x}}$.

Proposition 4 (Moments of \mathbf{y}). The approximate⁴ mean and covariance of $\mathbf{y}[k]$ can be determined by combining the results from Proposition 2 or Propositions 3 with the additional uncertainty introduced by channel noise according to

$$\hat{\boldsymbol{\mu}}_{\mathbf{y}[k]|C} = \boldsymbol{\mu}_{\bar{\mathbf{y}}[k]|C} + \mathbb{E}_{\text{UT}} \left\{ \mathbf{n}^{\text{C}} | \boldsymbol{\mu}_{\bar{\mathbf{y}}[k]|C}, \mathbf{C}_{\bar{\mathbf{y}}[k]|C} \right\} \quad (16a)$$

$$\hat{\mathbf{C}}_{\mathbf{y}[k]|C} = \mathbf{C}_{\bar{\mathbf{y}}[k]|C} + \text{COV}_{\text{UT}} \left\{ \mathbf{n}^{\text{C}} | \boldsymbol{\mu}_{\bar{\mathbf{y}}[k]|C}, \mathbf{C}_{\bar{\mathbf{y}}[k]|C} \right\}, \quad (16b)$$

where $C \in \{\mathbf{s}[k], \mathcal{S}(s[k])\}$. The statistics of $\mathbf{n}^{\text{C}}(\bar{\mathbf{y}}[k])$ can be tedious to derive for signal-dependent noise but are easily estimated using the UT as described in Section III-C. For a solution via integration over conditional pdfs, we refer the reader to [1].

Proof for (16a). Exploiting the linearity of the expectation operator and (1c) yields

$$\begin{aligned} \boldsymbol{\mu}_{\mathbf{y}[k]|C} &= \mathbb{E} \{ \bar{\mathbf{y}}[k] | C \} + \mathbb{E} \{ \mathbf{n}^{\text{C}}(\bar{\mathbf{y}}[k]) | C \} \\ &= \boldsymbol{\mu}_{\bar{\mathbf{y}}[k]|C} + \mathbb{E} \{ \mathbf{n}^{\text{C}}(\bar{\mathbf{y}}[k]) | C \}. \end{aligned}$$

⁴Note that we can only obtain approximations in the general case because we have only access to the mean and covariance of $\bar{\mathbf{y}}[k]$ but the full pdf of $\bar{\mathbf{y}}[k]$ would be required to obtain the exact mean and covariance of $\mathbf{n}^{\text{C}}(\bar{\mathbf{y}}[k])$.

Then, we exploit that $E \{ \mathbf{n}^C(\bar{\mathbf{y}}[k])|C \} \approx E_{\text{UT}} \{ \mathbf{n}^C | \boldsymbol{\mu}_{\bar{\mathbf{y}}[k]|C}, \mathbf{C}_{\bar{\mathbf{y}}[k]|C} \}$ because \mathbf{n}^C depends only on $\bar{\mathbf{y}}[k]$ which in turn depends only on C but there is no direct dependency of \mathbf{n}^C on C . Here, $\boldsymbol{\mu}_{\bar{\mathbf{y}}[k]|C}$ and $\mathbf{C}_{\bar{\mathbf{y}}[k]|C}$ are obtained from Proposition 2 or Proposition 3. \square

Proof for (16b). The proof is analogous to the proof for (16a). \square

Corollary 4.1 (SIN). *For SIN, we obtain the exact mean and covariance of $\mathbf{y}[k]$ as follows:*

$$\boldsymbol{\mu}_{\mathbf{y}[k]|C}^{\text{SIN}} = \boldsymbol{\mu}_{\bar{\mathbf{y}}[k]|C}^{\text{SIN}} + \boldsymbol{\mu}_{\mathbf{n}^C}^{\text{SIN}} \quad (17a)$$

$$\mathbf{C}_{\mathbf{y}[k]|C}^{\text{SIN}} = \mathbf{C}_{\bar{\mathbf{y}}[k]|C}^{\text{SIN}} + \mathbf{C}_{\mathbf{n}^C}^{\text{SIN}}. \quad (17b)$$

Proof. To obtain (17a), we insert $E \{ \mathbf{n}^C(\bar{\mathbf{y}}[k])|C \} = \boldsymbol{\mu}_{\mathbf{n}^C}^{\text{SIN}}$ into (16a). Analogously, we obtain (17b). \square

Corollary 4.2 (SDCN). *For SDCN, we obtain the mean of $\mathbf{y}[k]$ exactly and approximate the covariance using the UT:*

$$\boldsymbol{\mu}_{\mathbf{y}[k]|C}^{\text{SDCN}} = \boldsymbol{\mu}_{\bar{\mathbf{y}}[k]|C}^{\text{SIN}} \quad (18a)$$

$$\hat{\mathbf{C}}_{\mathbf{y}[k]|C}^{\text{SDCN}} = \mathbf{C}_{\bar{\mathbf{y}}[k]|C}^{\text{SIN}} + \text{Cov}_{\text{UT}} \{ \mathbf{n}^C | \boldsymbol{\mu}_{\bar{\mathbf{y}}[k]|C}, \mathbf{C}_{\bar{\mathbf{y}}[k]|C} \}. \quad (18b)$$

Proof. To obtain (18a), we observe that (3) is zero-mean according to

$$\begin{aligned} E \left\{ \left[\sqrt{\nu^C \mathbf{y}[k]} \right]_i \cdot [\bar{\mathbf{n}}]_i \right\} &= E \left\{ \left[\sqrt{\nu^C \mathbf{y}[k]} \right]_i \right\} \cdot E \{ [\bar{\mathbf{n}}]_i \} \\ &= E \left\{ \left[\sqrt{\nu^C \mathbf{y}[k]} \right]_i \right\} \cdot 0 = 0, \end{aligned}$$

where $i \in \{1, \dots, S\}$ and we exploited that the expectation of the product of two independent RVs is the product of their expectations. Eq. (18b) is obtained analogously to the proof for (16a). \square

Proposition 5 (Moments of \mathbf{z}). *Finally, we approximate the first- and second-order moments of $\mathbf{z}[k]$ for a given condition $C \in \{s[k], \mathcal{S}(s[k])\}$ using the UT as follows:*

$$\hat{\boldsymbol{\mu}}_{\mathbf{z}[k]|C} = \hat{\boldsymbol{\mu}}_{\mathbf{f}(\mathbf{y}[k])|C} + E_{\text{UT}} \left\{ \mathbf{n}^{\text{RX}} | \hat{\boldsymbol{\mu}}_{\mathbf{f}(\mathbf{y}[k])|C}, \hat{\mathbf{C}}_{\mathbf{f}(\mathbf{y}[k])|C} \right\} \quad (19a)$$

$$\hat{\mathbf{C}}_{\mathbf{z}[k]|C} = \hat{\mathbf{C}}_{\mathbf{f}(\mathbf{y}[k])|C} + \text{Cov}_{\text{UT}} \left\{ \mathbf{n}^{\text{RX}} | \hat{\boldsymbol{\mu}}_{\mathbf{f}(\mathbf{y}[k])|C}, \hat{\mathbf{C}}_{\mathbf{f}(\mathbf{y}[k])|C} \right\}. \quad (19b)$$

Proof. For both $\hat{\boldsymbol{\mu}}_{\mathbf{z}[k]|C}$ and $\hat{\mathbf{C}}_{\mathbf{z}[k]|C}$, we use the same steps: First, we estimate $\hat{\boldsymbol{\mu}}_{\mathbf{f}(\mathbf{y}[k])|C}$ and $\hat{\mathbf{C}}_{\mathbf{f}(\mathbf{y}[k])|C}$ using the UT with the (approximate) mean and covariance from Proposition 4 or one of the relevant corollaries as input to the UT. Then, we continue analogously to the proof of (16a) for the final expression. \square

Corollary 5.1 (SIN, SDCN). *For signal-independent RX noise, these expressions simplify to:*

$$\hat{\boldsymbol{\mu}}_{\mathbf{z}[k]|C} = \hat{\boldsymbol{\mu}}_{\mathbf{f}(\mathbf{y})|C} + \boldsymbol{\mu}_{\mathbf{n}^{\text{RX}}}^{\text{SIN}} \quad (20a)$$

$$\hat{\mathbf{C}}_{\mathbf{z}[k]|C} = \hat{\mathbf{C}}_{\mathbf{f}(\mathbf{y})|C} + \mathbf{C}_{\mathbf{n}^{\text{RX}}}^{\text{SIN}}. \quad (20b)$$

Proof. We use the general formulation for the moments of $\mathbf{z}[k]$ and then continue analogously to the proofs for Corollary 4.1. \square

E. Obtaining the Final Moments

Finally, we show how the different propositions, and their respective corollaries, can be combined to obtain the first- and second-order moments utilized by the various proposed detectors. For the ISI-unaware detector, we exploit Propositions 1, 2, 4, and 5, while setting $\kappa^{\max} = 0$. For the LC detector, we exploit Propositions 1, 3, 4, and 5 using a κ^{\max} appropriate for the channel. The sequence detector uses the same propositions like the LC detector, only Proposition 3 is replaced by Proposition 2.

IV. MOMENT-BASED MIXTURE ALPHABET DESIGN

In the previous section, we introduced several detectors for a given mixture alphabet. Now, in Section IV-A, we develop a systematic approach to generate such alphabets, before introducing an adaptive transmission scheme in Section IV-B.

A. Static Mixture Alphabet Design

Existing schemes for designing signal constellations usually made idealizing assumptions about the RX characteristics, e.g., the ability to count individual molecules [38], or consider only a specific type of RX [17]. In contrast, here, we propose an algorithm for mixture design that is applicable to general RXs with non-linear, cross-reactive, and noisy sensing units. In this general setting, the identification of *optimal* alphabets, i.e., alphabets that achieve minimal SERs, is usually infeasible. Thus, we instead propose a suboptimal, greedy approach, summarized in Algorithm 2, that optimizes the pair-wise separability of the symbols in the SOD. While the algorithm has been developed for ISI-free scenarios, it can also be applied in ISI scenarios, particularly in combination with the sequence detector introduced in Section III-B3⁵.

Our approach can be divided into an initialization stage during which the first symbol is chosen and into an iteration stage during which the remaining symbols are added one by one until \mathcal{A} contains the desired number of elements, N . During the **initialization stage**, we choose an initial point \mathbf{i}_0 that is drawn from the uniform distribution over the feasible set \mathcal{F}_x (line 3) and we create a candidate set \mathcal{C} whose $|\mathcal{C}|$ elements are uniformly distributed in \mathcal{F}_x (line 4). Then, we select the candidate with the largest distance to \mathbf{i}_0 as measured by some distance metric $d(\cdot, \cdot)$, which we will introduce below, as the first symbol (line 5). This procedure ensures that the first

⁵Designing a mixture alphabet explicitly for ISI scenarios is challenging because all symbols are indirectly coupled through their contribution to the ISI. However, the proposed algorithm finds a mixture alphabet that is also suitable for ISI channels.

Algorithm 2 Static Mixture Alphabet Design Algorithm

- 1: **Initialization**
 - 2: Initialize symbol alphabet: $\mathcal{A} = \{\}$
 - 3: Generate initial point: $\mathbf{i}_0 \sim \mathcal{U}(\mathcal{F}_x)$
 - 4: Generate candidate set \mathcal{C} : $\mathbf{c} \sim \mathcal{U}(\mathcal{F}_x), \forall \mathbf{c} \in \mathcal{C}$
 - 5: Add initial signal point: $\mathcal{A} = \mathcal{A} \cup \{\arg \max_{\mathbf{c} \in \mathcal{C}} d(\mathbf{c}, \mathbf{i}_0)\}$
 - 6: **Iteration**
 - 7: **while** $|\mathcal{A}| \leq N$ **do**
 - 8: Add signal point: $\mathcal{A} = \mathcal{A} \cup \{\arg \max_{\mathbf{c} \in \mathcal{C}} \min_{\bar{\mathbf{x}} \in \mathcal{A}} d(\mathbf{c}, \bar{\mathbf{x}})\}$
 - 9: **end while**
-

symbol will usually lie somewhere close to the boundary of \mathcal{F}_x and not in the middle of \mathcal{F}_x , which could impair the overall quality of the mixture alphabet. Then, during the **iteration stage** (lines 6-9), we add one new symbol per iteration until the full mixture alphabet is constructed. In each iteration, the candidate with the largest minimum distance to any existing symbol in \mathcal{A} is selected. The quality of the constructed mixture alphabet is determined by the size of the candidate set $|\mathcal{C}|$ and the chosen distance metric. Thus, we introduce two distance metrics below.

Both metrics utilize the approximate first- and second-order moments of $\mathbf{z}[k]$ that are computed using Propositions 1, 3, 4, and 5 while setting $\kappa^{\max} = 0$, i.e., analogous to the ISI-unaware detector. An obvious choice for $d(\cdot, \cdot)$ is the **Euclidean distance** between the mean values of the two mixtures $\bar{\mathbf{x}}_i$ and $\bar{\mathbf{x}}_j$ in the SOD, i.e.,

$$d^{\ell_2}(\bar{\mathbf{x}}_i, \bar{\mathbf{x}}_j) = \|\hat{\boldsymbol{\mu}}_{\mathbf{z}|\bar{\mathbf{x}}_i} - \hat{\boldsymbol{\mu}}_{\mathbf{z}|\bar{\mathbf{x}}_j}\|_2. \quad (21)$$

Alternatively, to account for non-uniform signal spread, we can use the distance metric incorporating the symbols' covariances that was introduced in [17] as a **generalization of the SNR** to mixture communications. Specifically, this metric increases with the Euclidean distance between the mean values of the two symbols, but it decreases with increasing variance along the shortest path between the mean values. Formally, the metric is given by

$$d^{\text{SNR}}(\bar{\mathbf{x}}_i, \bar{\mathbf{x}}_j) = \frac{\|\hat{\boldsymbol{\mu}}_{\mathbf{z}|\bar{\mathbf{x}}_i} - \hat{\boldsymbol{\mu}}_{\mathbf{z}|\bar{\mathbf{x}}_j}\|_2^2}{\mathbf{p}^T \hat{\mathbf{C}}_{\mathbf{z}|\bar{\mathbf{x}}_i} \mathbf{p} + \mathbf{p}^T \hat{\mathbf{C}}_{\mathbf{z}|\bar{\mathbf{x}}_j} \mathbf{p}} \quad (22)$$

where $\mathbf{p} = \frac{\hat{\boldsymbol{\mu}}_{\mathbf{z}|\bar{\mathbf{x}}_i} - \hat{\boldsymbol{\mu}}_{\mathbf{z}|\bar{\mathbf{x}}_j}}{\|\hat{\boldsymbol{\mu}}_{\mathbf{z}|\bar{\mathbf{x}}_i} - \hat{\boldsymbol{\mu}}_{\mathbf{z}|\bar{\mathbf{x}}_j}\|_2}$. While computationally more complex, $d^{\text{SNR}}(\cdot, \cdot)$ promises a higher performance compared to $d^{\ell_2}(\cdot, \cdot)$ due to the consideration of the covariances of both symbols.

B. Adaptive Alphabet Design - Chemical Precoding

In addition to the algorithm for the design of static mixture alphabets, we also propose an adaptive transmission scheme where the TX determines in each interval which concentration

vector $\bar{\mathbf{x}}[k]$ to transmit. This scheme assumes that the RX employs an LC detector trained on a static mixture alphabet \mathcal{A} generated by Algorithm 2. Then, the RX chooses the mixture $\bar{\mathbf{x}}[k]$ so that the resulting mixture at the RX is close to $\boldsymbol{\mu}_{\mathbf{y}[k]|S(s[k])}$ for the desired symbol $s[k]$. This corresponds to a form of precoding known in wireless communication.

Algorithm 3 Adaptive Transmission Scheme

- 1: **Initialization:**
 - 2: Generate candidate set \mathcal{C} : $\mathbf{c} \sim \mathcal{U}(\mathcal{F}_x)$, $\forall \mathbf{c} \in \mathcal{C}$
 - 3: Compute $\boldsymbol{\mu}_{\mathbf{x}|\mathbf{c}}$ using Proposition 1 $\forall \mathbf{c} \in \mathcal{C}$
 - 4: **Symbol Transmission:**
 - 5: **for** $k \in \mathbb{N}_{\geq 0}$ **do**
 - 6: Compute ISI: $\mathbf{y}^{\text{ISI}}[k] = \sum_{\kappa=1}^{\kappa^{\text{max}}} \mathbf{H}[\kappa] \boldsymbol{\mu}_{\mathbf{x}|\mathbf{c}[k-\kappa]}$
 - 7: Ideal mixture: $\mathbf{x}^{\text{ideal}}[k] = \mathbf{H}^{-1}[0] \cdot \text{proj}_{\mathcal{F}_x} (\boldsymbol{\mu}_{\mathbf{y}|S(s[k])} - \mathbf{y}^{\text{ISI}}[k])$
 - 8: Select best candidate: $\mathbf{c}[k] = \arg \min_{\mathbf{c} \in \mathcal{C}} \|\boldsymbol{\mu}_{\mathbf{x}|\mathbf{c}} - \mathbf{x}^{\text{ideal}}[k]\|_2$
 - 9: **end for**
-

Our approach, summarized in Algorithm 3, can be divided into an initialization stage and into the actual symbol transmission. During the **initialization stage**, we create a candidate set \mathcal{C} whose $|\mathcal{C}|$ elements are uniformly distributed in \mathcal{F}_x (line 2), and then we compute for each candidate, $\mathbf{c} \in \mathcal{C}$, $\boldsymbol{\mu}_{\mathbf{x}|\mathbf{c}}$ using Proposition 1 (line 3). During **symbol transmission**, we adaptively compute the expected ISI caused by the previously transmitted mixtures (line 6) according to

$$\mathbf{y}^{\text{ISI}}[k] = \sum_{\kappa=1}^{\kappa^{\text{max}}} \mathbf{H}[\kappa] \boldsymbol{\mu}_{\mathbf{x}|\mathbf{c}[k-\kappa]}, \quad (23)$$

where $\mathbf{c}[k-\kappa]$ denotes the mixture released κ intervals ago. Then, in line 7, we identify which mixture should be transmitted over the channel so that the resulting mixture at the RX is closest to the mixture lying in the center of the decision region for $s[k]$ according to

$$\mathbf{x}^{\text{ideal}}[k] = \mathbf{H}^{-1}[0] \cdot \text{proj}_{\mathcal{F}_x} (\boldsymbol{\mu}_{\mathbf{y}|S(s[k])} - \mathbf{y}^{\text{ISI}}[k]), \quad (24)$$

where $\text{proj}_{\mathcal{F}_x}(\cdot)$ projects a point onto \mathcal{F}_x . This is necessary to account for the possibility that a non-realizable concentration would be ideal. Then, we instead select the candidate \mathbf{c} whose $\boldsymbol{\mu}_{\mathbf{x}|\mathbf{c}}$ is closest to $\mathbf{x}^{\text{ideal}}[k]$ (line 8). It should be noted that the proposed algorithm is computationally very inexpensive as we do not propagate mixtures through $\mathbf{f}(\cdot)$ and the *nearest-neighbor search* in line 8 can be efficiently implemented, e.g., via k-d trees [39], [40].

TABLE I: Default system parameters for the simulations.

Parameter	Value (SIN)	Value (SDCN)	Parameter	Value (SIN)	Value (SDCN)
R	3		S	2	
$\mathbf{H}[\kappa]$	[0.01 · \mathbf{I} , 0.0025 · \mathbf{I} , 0.0005 · \mathbf{I}]		$ \mathcal{C} $	500	
$\boldsymbol{\mu}_{\mathbf{n}^{\text{TX}}}$	$\mathbf{0}$		$\mathbf{C}_{\mathbf{n}^{\text{TX}}}$	$10^6 \cdot \mathbf{I}$	
$\boldsymbol{\mu}_{\mathbf{n}^{\text{C}}}$	$10 \cdot \mathbf{1}$	-	$\mathbf{C}_{\mathbf{n}^{\text{C}}}$	$10 \cdot \mathbf{I}$	-
$\boldsymbol{\mu}_{\mathbf{n}^{\text{RX}}}$	$\mathbf{0}$		$\mathbf{C}_{\mathbf{n}^{\text{RX}}}$	$10^{-13} \cdot \mathbf{I}$	
$\mathcal{F}_{\mathbf{x}}$ (no ISI)	[0, 4 · 10 ⁴] ^S		$\mathcal{F}_{\mathbf{x}}$ (ISI)	[0, 3 · 10 ⁴] ^S	
$\mathcal{F}_{\mathbf{x}}$ (TGS)	[20 · 10 ³ , 10 · 10 ⁴] × [15 · 10 ³ , 50 · 10 ³]			-	

V. PERFORMANCE EVALUATION

In this section, we present simulation results for the different detectors proposed in Section III, the mixture alphabet design algorithm proposed in Section IV-A, and the adaptive transmission scheme proposed in Section IV-B.

A. Simulation Setup

We provide simulations for both the SIN and SDCN scenarios in conjunction with the non-linear model of an array of MOS sensors. We parametrize the model for MOS sensors in two ways: First, to demonstrate the necessity of explicitly accounting for the non-linear behavior of sensors, we fit the model to measurement data for two commercially available MOS sensors (TGS800 and TGS826) responding to mixtures of ethanol and ammonia [31]. For our further experiments, on the other hand, we generate artificial sensor data as detailed in Appendix A to allow for a more general investigation into the importance of accounting for the RX characteristics, e.g., to investigate how the number of employed sensors affects communication performance. Relevant simulation parameters are reported in Table I. To vary the noise power, and thus the SNR, we multiply all covariance matrices by a common factor ν and set $\nu^{\text{C}} = \nu$. Note that we show SERs in result plots as a function $1/\nu$ analogously to showing SERs over the SNR in wireless communications.

B. Detector Analysis

In the following, we first motivate the explicit consideration of non-linear, cross-reactive RX behavior before evaluating the performance of our proposed detectors quantitatively.

1) *ISI-free Scenario*: Before starting the systematic evaluation of the proposed detectors, we first provide some intuition **why it is important to account for the characteristics of the RX array**. To this end, we employ an alphabet with $N = 6$ symbols optimized for an array of the two considered TGS sensors in the SIN scenario⁶. In Figure 2, we show on the left and in the

⁶Here, we use noise parameters deviating from the ones reported in Table I to get more informative results for the chosen sensors. Specifically, we use $\boldsymbol{\mu}_{\mathbf{n}^{\text{TX}}} = \mathbf{0}$, $\mathbf{C}_{\mathbf{n}^{\text{TX}}} = \mathbf{0}$, $\boldsymbol{\mu}_{\mathbf{n}^{\text{C}}} = 10 \cdot \mathbf{1}$, $\mathbf{C}_{\mathbf{n}^{\text{C}}} = 10 \cdot \mathbf{I}$, and $\boldsymbol{\mu}_{\mathbf{n}^{\text{RX}}} = \mathbf{0}$, $\mathbf{C}_{\mathbf{n}^{\text{RX}}} = 10^{-12} \cdot \mathbf{I}$.

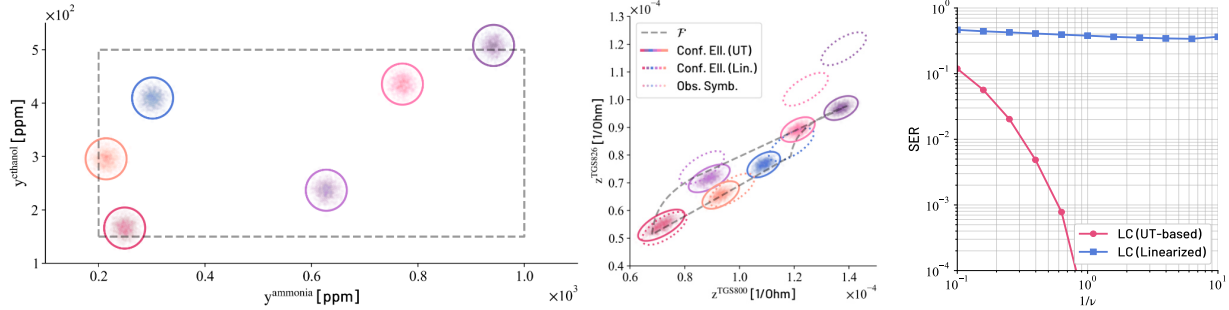


Fig. 2: **Impact of non-linear, cross-reactive sensor behavior.** The UT-based detectors capture the likelihoods of $y[k]$ (left) and of $z[k]$ (center). On the other hand, the sensor responses predicted by the linearized sensor models (center, dashed lines) differ systematically from the actual sensor responses (center plot, dots). This is also reflected in the respective SERs of the UT-based detector (right, purple) and the detector relying on a linearized sensor model (right, blue).

middle respectively the empirical likelihoods of $y[k]$ and $z[k]$ (colored dots) together with the 3σ -confidence ellipses obtained from the moments used by the UT-based detectors (solid lines). For $z[k]$, we additionally show the 3σ -confidence ellipses obtained from a linearized $f(\cdot)$ (dashed lines), i.e., from the first-order two-dimensional Taylor-expansion of $f(\cdot)$ around the center of the feasible set. Clearly, the moments based on the UT match the empirical likelihoods very closely even for $z[k]$. On the other hand, the moments for the linearized sensor function do not match the empirical likelihoods. This is also reflected in the SERs of the UT-based detector and the detector relying on a linearized sensor model, as shown on the right-hand side of Figure 2. While the SER of the UT-based detector is approx. 10% for $1/\nu = 10^{-1}$ and decreases with increasing $1/\nu$, the detector relying on the linearized system model suffers from SERs of at least 20% independent of the SNR.

In the following, we analyze the **quantitative performance** of the detectors proposed in Section III using artificial sensor arrays that are generated as described in Appendix A. To this end, we compare our UT-based detectors to two baselines, namely the *centroid detector* and *k-nearest-neighbor (kNN) classifiers*, which we describe in the following in more detail.

The **centroid detector** is a UT-based detector but with $\hat{\mathbf{C}}_{z[k]|s[k]} = \mathbf{I}$, $\forall s[k] \in \mathcal{S}_0$, i.e., only the mean - or centroid - of the likelihoods is considered. While this introduces some sub-optimality compared to the UT-based detector which considers the spread of the individual symbols, it has an even lower computational complexity during symbol detection as only the computation of ℓ_2 distances is necessary. Thus, the centroid detector may be suitable for scenarios with very strict hardware and complexity constraints at the RX. Furthermore, we consider an **kNN classifier**, which is a commonly used *model-free* approach in machine learning, where new samples are

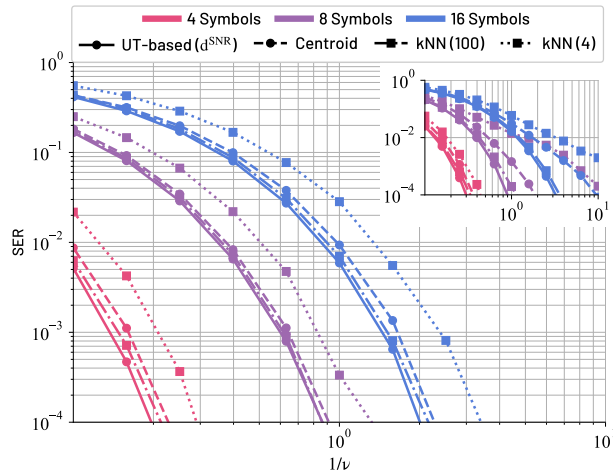


Fig. 3: **Detector Comparison for ISI-free scenarios.** The UT-based detector with the covariance-aware distance metric (solid) consistently achieves the lowest SERs compared to centroid detector (dashed) and kNN detectors (dashed-dotted, dotted).

classified according to the classes of the k nearest samples in terms of the Euclidean distance. While this approach has the advantage of not requiring any system model, and instead uses real-world measurements (or simulations), its performance depends on the number of training samples whose generation might be costly if they are obtained from measurements. Furthermore, the complexity during the online phase also increases with the number of training samples, yielding a non-trivial accuracy-complexity trade-off. Thus, we consider kNN classifiers trained with four samples per symbol, i.e., the same number of evaluations of $f(\cdot)$ during the offline phase as for the UT-based detector, and with 100 samples per symbol, respectively.

Figure 3 presents the SER achieved by the UT-based detectors and the aforementioned baselines for 4, 8, and 16 symbols as a function of $1/\nu$ for given mixture alphabets in the SIN scenario⁷. First, we observe that the SER decreases as $1/\nu$ increases for all considered detectors. Our proposed UT-based detector achieves the lowest SER for all ν although the kNN detector with 100 training samples per symbol exhibits almost the same performance at the cost of requiring much more training samples. The kNN detector with only four training samples per symbol has significantly worse performance than all other schemes, demonstrating that a model-based approach, such as the proposed UT-based detector, can achieve significantly higher *sample efficiency* compared to purely data-driven approaches, i.e., a lower number of training samples is needed to achieve a desired performance. As expected, the centroid detector has some performance loss compared to the UT-based detector since it neglects the spread of the likelihoods. Both the centroid detector and the kNN detector with four training samples perform

⁷We show the results for the SDCN scenario as inset to Figures 3, 4, and 5. Since similar trends can be observed for both SIN and SDCN, we focus our discussion on the SIN case for brevity and highlight only the differences.

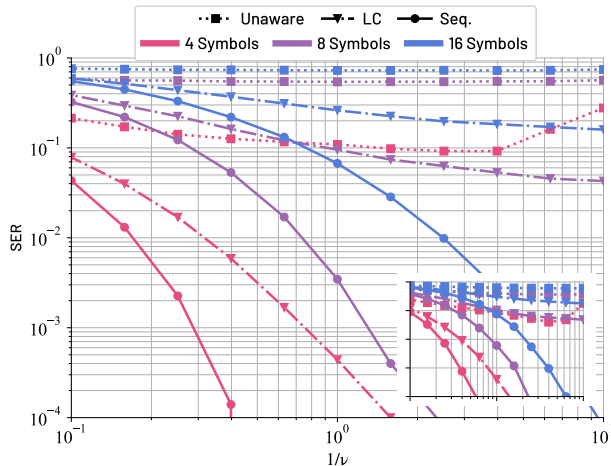


Fig. 4: **Detector Comparison for ISI scenarios.** The ISI-unaware detector (dashed) makes systematic decision errors, causing unacceptable SERs for all SNRs and alphabet sizes. The LC (dashed-dotted) detector improves the performance but still cause high SERs for higher numbers of symbols, whereas the sequence detector (solid) yields fast SER decays with increasing SNR.

worse for SDCN than for SIN. This is due to the non-uniform signal-spread caused by SDCN: The centroid detector does not account for such non-uniform signal spread by design and the kNN detector is not able to model the likelihoods appropriately with only four training samples.

In summary, Figure 3 illustrates that the **UT-based detector achieves a lower SER** than the two baseline methods, confirming its applicability in settings with significant non-linear and cross-reactive RX characteristics. At the same time, the UT-based detector requires, in comparison to the data-driven baseline, significantly fewer training samples for a given performance.

2) *ISI Scenario:* In the following, we investigate the performance of the proposed detectors when there is significant ISI. Figure 4 shows the SERs achieved by the proposed detectors as a function of $1/\nu$. The mixture alphabet optimized for one instance of the artificial sensor array in the SIN scenario is adopted.

First, we observe that the ISI-unaware detector (dotted line) yields an unacceptably high SER in all cases: Even when $|\mathcal{S}_0| = 4$, it barely achieves an SER below 10%, independent of the SNR. This is because $\mathbb{E}\{y[k]\}$ shifts compared to the ISI-free case due to the additional ISI molecules in the channel, causing a systematic mismatch between the expected and the actual sensor outputs⁸. On the other hand, the LC detector achieves lower SERs that decrease with increasing SNRs. Finally, we observe that the **sequence detector achieves the lowest SER** of all proposed detectors. Its relative advantage over the symbol-by-symbol detectors increases with

⁸In the scenario with 4 symbols, the SER of the ISI-unaware detector increases again for high SNRs because the SNR-specific detector calibration leads to changing decision regions. For 8 and 16 symbols, the SER is, independent of the SNR, so high that the effect does not become visible.

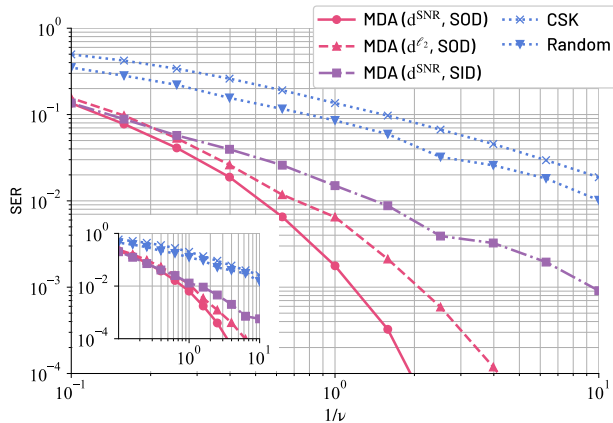


Fig. 5: **Comparison of Mixture Design Algorithms for ISI-free scenarios.** The SER of mixture alphabets in the SOD with the SNR-based distance metric (pink solid) is consistently lower than that of alphabet designs in the SID (purple) and baselines like CSK or random alphabets (blue).

increasing SNR and increasing alphabet size. This matches the insights from Remark 3: The signal spread due to ISI is usually much higher than the spread caused by noise. As the SNR increases, the spread due to noise decreases while the spread due to ISI remains almost constant, explaining the growing advantage of the sequence detector which can exploit information from previous intervals to reduce the uncertainty about the ISI.

C. Mixture Alphabet Design Analysis

So far, we have established that accounting for the non-linear, cross-reactive behavior of the RX sensor array is important for effective detection. In the following, we focus on the performance of the proposed mixture alphabet design algorithm and the adaptive transmission scheme.

1) *Mixture Alphabet Design Algorithm:* In Figure 5, we evaluate the mixture alphabets created by the algorithm proposed in Section IV-A for both $d^{\text{SNR}}(\cdot, \cdot)$ and $d^{\ell_2}(\cdot, \cdot)$. To this end, we compare the optimized designs to several baselines for $N = 8$ with regard to the SER achieved by the UT-based detectors as performance metric. In our simulations, we average over 100 different RX arrays that are generated as described in Appendix A to get generalizable insights.

As a first baseline, we use **Algorithm 2 in the SID**, i.e., we compute $d^{\text{SNR}}(\cdot, \cdot)$ for the approximate likelihoods of \mathbf{y} instead of \mathbf{z} and thus do not account for the non-linear, cross-reactive RX behavior during mixture design. As a second baseline, we consider **CSK with equally spaced constellation points** for one of the two signaling molecules in \mathcal{F}_x . This helps to quantify the gain that can be achieved by allowing a second dimension for the mixture design. Finally, we also consider a **random mixture design**, where the individual symbols are simply drawn independently from $\mathcal{U}(\mathcal{F}_x)$.

In Figure 5, we compare the proposed MDA to the aforementioned baselines for SIN. As expected, our MDA with $d^{\text{SNR}}(\cdot, \cdot)$ achieves the lowest SER for a given value of $1/\nu$. Using

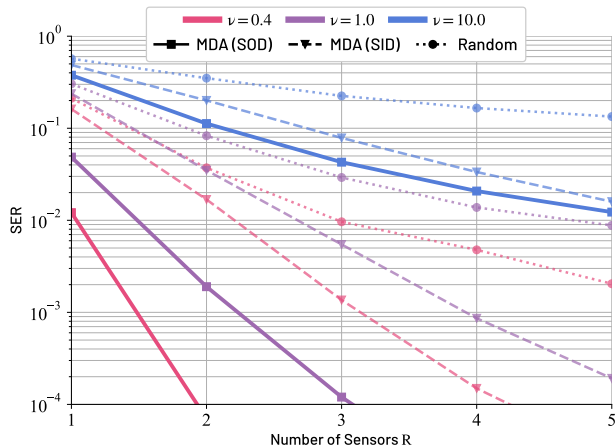


Fig. 6: **Impact of the optimization domain for different numbers of sensors.** As the number of sensors increases, the SER decreases for all alphabet design algorithms and optimization domains. The SOD-based optimization (solid) achieves the lowest SER compared to SID-based optimization (dashed) and random alphabets (dotted).

$d^{\ell_2}(\cdot, \cdot)$ entails slightly lower computational complexity, but is also subject to performance loss relative to $d^{\text{SNR}}(\cdot, \cdot)$. Regardless of the employed distance metric, our algorithm outperforms all baselines, including the mixture design in the SID which does not account for the non-linear, cross-reactive RX behavior⁹. However, the advantage of the proposed algorithm compared to optimization in the SID is less pronounced for low SNRs, which we attribute to the fact for low SNRs that the likelihoods are less accurately described by only the first- and second-order moments when feeding them through $\mathbf{f}(\cdot)$: As the spread of $\mathbf{y}[k]$ increases, $p_{\mathbf{z}[k]|s[k]}(\mathbf{z}[k])$ may be less accurately described by a Gaussian distribution than for a smaller spread of $\mathbf{y}[k]$, where $\mathbf{f}(\cdot)$ can be locally approximated as linear. Such a mismatch can lead to scenarios, where optimization in the SID can yield similar performance to optimization in the SOD.

Finally, we examine how the number of available sensors affects which optimization domain is preferable. We investigate this in Figure 6, where we use $N = 8$, $S = 3$, and vary R from 1 to 5. As before, the sensor arrays are generated as described in Appendix A. All remaining system parameters are kept at their default values for the SIN scenario. When comparing the SERs of the alphabets generated by the proposed MDA in the SOD, the proposed MDA in the SID, and randomly, we observe that the SER decreases as R increases for all considered alphabets. This is expected as more independent observations of $\mathbf{y}[k]$ become available as R increases. We can observe that, in the considered scenario, optimization in the SOD can, depending on the SNR, achieve the same SER as optimization in the SID with one or two sensors less. In summary,

⁹Note that CSK is outperformed here even by random mixture design. This is because we average over 100 RX arrays and some of those arrays are not sensitive to the molecule type employed by CSK. By exploiting both molecule types, random mixture design is robust against this effect.

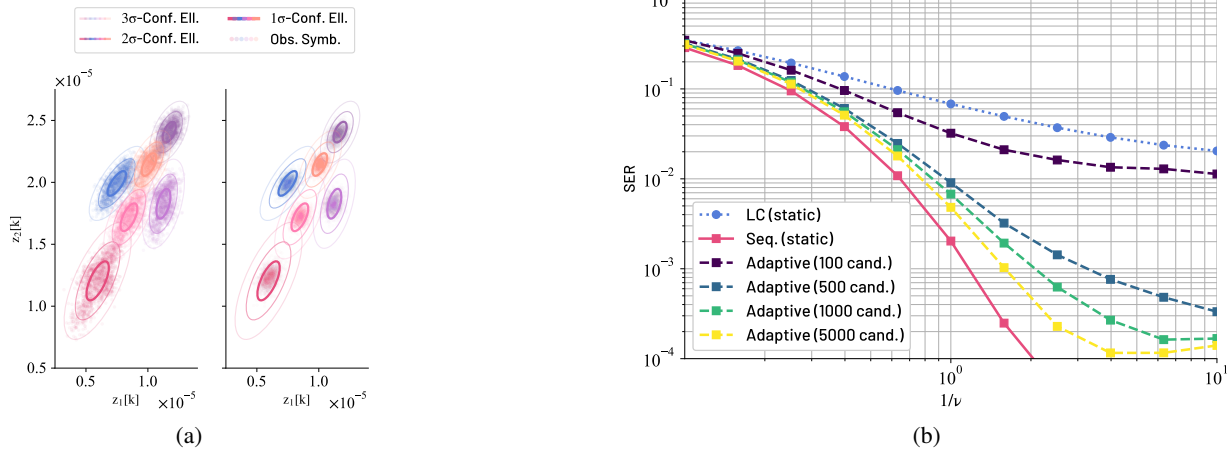


Fig. 7: **Adaptive Transmission Scheme.** (a) The sensor outputs of the adaptive transmission scheme (right) are more concentrated in the center of the LC's decisions region compared to the static alphabet (left). (b) The adaptive scheme (dashed) outperforms the LC detector (dotted) and approaches the performance of the sequence detector (solid).

Figures 5 and 6 shows that **RX-aware mixture design can enable lower SERs** than simply optimizing for separable molecule concentrations.

2) *ISI Scenario:* We have already shown in Section V-B2 that the alphabets generated by the MDA enable low SERs also for channels with ISI, especially when combined with the sequence detector proposed in Section III-B3. Now, we examine the performance of the **adaptive transmission scheme** proposed in Section IV-B and its ability to enable low SERs when combined with the LC symbol-by-symbol detector, thus reducing the required computational complexity at the RX. To illustrate the working principle of the adaptive scheme, we consider an array with $R = 2$ sensors and an alphabet of size $N = 6$, generated by the proposed MDA. In Figure 7a, we show the sensor outputs for the static alphabet on the left-hand side and the sensor outputs for the adaptive transmission scheme on the right-hand side. Additionally, we show confidence ellipses of the LC by solid lines in each plot, where the opacity increases from the 1 σ to the 3 σ confidence ellipse. This figure reveals why the adaptive transmission scheme can achieve lower SERs: The sensor outputs are much more tightly packed in the center of the decision regions when employing the adaptive transmission scheme, enabling a much lower SER compared to the static mixture alphabet. This becomes apparent in Figure 7b, where we investigate the achieved SER. Specifically, we compare the proposed adaptive scheme to a static mixture alphabet, the latter in conjunction with either the LC detector (blue dotted) or the sequence detector (red solid). The dashed lines show the SER achieved by the adaptive transmission scheme for different $|\mathcal{C}|$. As expected, increasing $|\mathcal{C}|$ decreases the SER and closes the gap between the LC and the sequence detector for low and moderate SNRs. Only for very high SNRs, the adaptive transmission scheme has an error-floor due to the finite $|\mathcal{C}|$ and, depending

on the scenario, because the released concentrations are confined to \mathcal{F}_x . In summary, Figure 7b shows that the proposed **adaptive transmission scheme enables low SERs in ISI channels** even when deploying LC symbol-by-symbol detectors at the RX.

VI. CONCLUSION

In this work, we studied the detection and alphabet design for molecule mixture communications for ISI channels and non-linear, cross-reactive RX arrays. Specifically, we proposed a comprehensive system model that accounts for release, propagation, and sensor noise and includes a non-linear, cross-reactive RX array. We then proposed a symbol-by-symbol detector that exploits statistical knowledge of the ISI and a sequence detector for static molecule mixture alphabets. Furthermore, we proposed a complementary mixture alphabet design algorithm that explicitly accounts for the employed RX and optimizes the separability of the sensor outputs of different symbols. We demonstrated via extensive simulations for ISI-free scenarios that our proposed detectors outperform data-driven baseline schemes and that our mixture alphabet design algorithm improves upon schemes that ignore the RX characteristics. We also verified that the sequence detector enables effective symbol detection even in scenarios with strong ISI. If the RX has extremely limited computational capacity, an adaptive transmission scheme can be employed in conjunction with a symbol-by-symbol detector to achieve similar performance as the sequence detector. Our results highlight that reliable communication is possible with non-linear, cross-reactive sensing units even in the presence of strong ISI. Potential future directions include the experimental validation of the proposed schemes, their extension to incorporate uncertainty regarding system parameters, e.g., due to factors like changes in temperature or humidity, and their extension to multi-user scenarios.

APPENDIX GENERATION OF ARTIFICIAL SENSOR DATA

While the response of MOS sensors to individual gases in clean background air is usually reported in the datasheets of those sensors, their response to mixtures is usually not reported in a way that can be used to parametrize (2). Also, sensor parameters are rarely reported in the literature and vary over several orders of magnitude depending on source and system parameters (see, e.g., [29], [31], [32]). Due to this lack of reliable data, we generate artificial sensor data that resembles the sensor parameters reported in [29]¹⁰. To this end, we perform

¹⁰It should be noted that some numerical values reported in [29, Table 1 & 2] seem inconsistent. For example, parameter A_i for sensor TGS822 is off by a factor of 10 compared to the results reported in Figure 6. Since it is not possible to check all the possible values, we decided to generate artificial data with similar characteristics instead of relying on the individual numbers.

rejection sampling, i.e., we generate the parameters for \mathbf{a} , \mathbf{A} , and \mathbf{b} independently and then check whether the joint parameter configuration for the sensor function $\mathbf{f}(\cdot)$ is valid, as will be defined below. Invalid configurations are disregarded and replaced by a new parameter set until a valid configuration is identified. A **valid sensor configuration** is monotonously increasing with increasing molecule concentrations throughout \mathcal{F}_y . This is evaluated by checking that $[\nabla_y \mathbf{f}(\mathbf{y})]_i \geq 0, \forall i \in \{0, \dots, S\}$, holds for 10^5 test points $\mathbf{y} \sim \mathcal{U}(\mathcal{F}_y)$. We select the **sensor parameters** independently for each species according to $\mathbf{a} \sim 10^{n_a}$, $\mathbf{A} \sim 10^{n_A}$, and $\mathbf{b} \sim \text{TruncNorm}(0.5, 0.2, [0.3, 0.7])$. Here, n_a is normal distributed with mean -6.5 and standard deviation 0.5 , and n_A is normal distributed with mean -7.5 and standard deviation 1 . $\text{TruncNorm}(0.5, 0.2, [0.3, 0.7])$ denotes a normal distribution with mean 0.5 and standard deviation 0.2 while being limited to the interval $[0.3, 0.7]$, thereby capturing the range of power law coefficients reported in the literature (see, e.g., [11], [30], [41]).

REFERENCES

- [1] B. Heinlein *et al.*, “Molecule mixture detection and alphabet design for non-linear, cross-reactive receiver arrays in MC,” in *Proc. 12th Ann. ACM Int. Conf. Nanoscale Comput. Commun.*, pp. 15–21, 2025.
- [2] W. Guo *et al.*, “Molecular physical layer for 6G in wave-denied environments,” *IEEE Commun. Mag.*, vol. 59, pp. 33–39, May 2021.
- [3] A. W. Eckford, “Achievable information rates for molecular communication with distinct molecules,” in *Proc. IEEE Bio-Inspired Models Netw. Inf. Comput. Syst.*, pp. 313–315, 2007.
- [4] X. Chen, Y. Huang, L.-L. Yang, and M. Wen, “Generalized molecular-shift keying (GMoSK): Principles and performance analysis,” *IEEE Trans. Mol. Biol. Multi-Scale Commun.*, vol. 6, no. 3, pp. 168–183, 2020.
- [5] M. O. Araz *et al.*, “Ratio shift keying modulation for time-varying molecular communication channels,” *IEEE Trans. Nanobiosci.*, vol. 23, pp. 176–189, Jan. 2024.
- [6] B. A. Kilic and O. B. Akan, “Multi ratio shift keying (MRSK) modulation for molecular communication,” *IEEE Trans. Commun.*, vol. 73, pp. 8873–8885, Oct. 2025.
- [7] Y. Tang, M. Wen, X. Chen, Y. Huang, and L.-L. Yang, “Molecular type permutation shift keying for molecular communication,” *IEEE Trans. Mol. Biol. Multi-Scale Commun.*, vol. 6, no. 2, pp. 160–164, 2020.
- [8] D. T. McGuinness *et al.*, “Experimental results on the open-air transmission of macro-molecular communication using membrane inlet mass spectrometry,” *IEEE Commun. Lett.*, vol. 22, pp. 2567–2570, Dec. 2018.
- [9] A. Wietfeld, S. Schmidt, and W. Kellerer, “Evaluation of a multi-molecule molecular communication testbed based on spectral sensing,” in *Proc. IEEE Glob. Commun. Conf.*, pp. 2102–2108, 2024.
- [10] V. Walter, D. Bi, D. L. R. Blanco, and Y. Deng, “CNN-based detection of mixed-molecule concentrations in molecular communication,” *arXiv preprint arXiv:2511.02105*, 2025.
- [11] N. Yamazoe and K. Shimano, “Theory of power laws for semiconductor gas sensors,” *Sens. Actuators B: Chem.*, vol. 128, pp. 566–573, Jan. 2008.
- [12] K. J. Albert *et al.*, “Cross-reactive chemical sensor arrays,” *Chem. Rev.*, vol. 100, pp. 2595–2626, June 2000.
- [13] F. Cali *et al.*, “Experimental implementation of molecule shift keying for enhanced molecular communication,” *IEEE Trans. Mol. Biol. Multi-Scale Commun.*, vol. 10, no. 1, pp. 175–184, 2024.
- [14] N.-R. Kim *et al.*, “An experimentally validated channel model for molecular communication systems,” *IEEE Access*, vol. 7, pp. 81849–81858, June 2019.
- [15] N. Farsad, W. Guo, and A. W. Eckford, “Tabletop Molecular Communication: Text Messages through Chemical Signals,” *PLoS ONE*, vol. 8, p. e82935, Dec. 2013.
- [16] S. Wisayataksin, P. Angkasuwan, and Y. Ariyakul, “4-ary odor-shift keying using multi-channel olfactory display,” in *Proc. 11th Int. Conf. Inf. Tech. El. Eng.*, pp. 1–4, 2019.

- [17] V. Jamali *et al.*, “Olfaction-inspired MCs: Molecule mixture shift keying and cross-reactive receptor arrays,” *IEEE Trans. Commun.*, vol. 71, pp. 1894–1911, Apr. 2023.
- [18] B. Tepekule, A. E. Pusane, H. B. Yilmaz, C.-B. Chae, and T. Tugcu, “ISI mitigation techniques in molecular communication,” *IEEE Trans. Mol., Biol., Multi-Scale Commun.*, vol. 1, pp. 202–216, June 2015.
- [19] D. Jing and A. W. Eckford, “Lightweight channel codes for ISI mitigation in molecular communication between bionanosensors,” *IEEE Sensors J.*, vol. 23, pp. 13859–13867, July 2023.
- [20] H. Arjmandi *et al.*, “ISI-avoiding modulation for diffusion-based molecular communication,” *IEEE Trans. Mol. Biol. Multi-Scale Commun.*, vol. 3, pp. 48–59, Mar. 2017.
- [21] V. Jamali, A. Ahmadzadeh, and R. Schober, “On the design of matched filters for molecule counting receivers,” *IEEE Commun. Lett.*, vol. 21, no. 8, pp. 1711–1714, 2017.
- [22] M. Kuran, H. B. Yilmaz, I. Demirkol, N. Farsad, and A. Goldsmith, “A survey on modulation techniques in molecular communication via diffusion,” *IEEE Commun. Surv. Tut.*, vol. 23, pp. 7–28, Jan. 2021.
- [23] W. Shin *et al.*, “Low-frequency noise in gas sensors: A review,” *Sens. Act. B: Chem.*, vol. 383, p. 133551, May 2023.
- [24] R. Hopper *et al.*, “Multi-channel portable odor delivery device for self-administered and rapid smell testing,” *Commun. Eng.*, vol. 3, p. 141, Oct. 2024.
- [25] S. Carkit-Yilmaz *et al.*, “Experimental analysis of surface-induced molecular adsorption in static airborne molecular communication environments,” in *Proc. 12th Ann. ACM Int. Conf. Nanoscale Comput. Commun.*, pp. 165–166, 2025.
- [26] J. Williams and A. Ringsdorf, “Human odour thresholds are tuned to atmospheric chemical lifetimes,” *Phil. Trans. Royal Soc. B*, vol. 375, no. 1800, p. 20190274, 2020.
- [27] N. Dennler *et al.*, “High-speed odor sensing using miniaturized electronic nose,” *Sci. Adv.*, vol. 10, p. eadp1764, Nov. 2024.
- [28] Y. Wu, M. Lei, and X. Xia, “Research progress of MEMS gas sensors: A comprehensive review of sensing materials,” *Sensors*, vol. 24, p. 8125, Dec. 2024.
- [29] E. Llobet *et al.*, “Steady-state and transient behavior of thick-film tin oxide sensors in the presence of gas mixtures,” *J. Electrochem. Soc.*, vol. 145, pp. 1772–1779, May 1998.
- [30] S. Madrolle, P. Grangeat, and C. Jutten, “A linear-quadratic model for the quantification of a mixture of two diluted gases with a single metal oxide sensor,” *Sens.*, vol. 18, p. 1785, June 2018.
- [31] S. Hirobayashi *et al.*, “Verification of a logarithmic model for estimation of gas concentrations in a mixture for a tin oxide gas sensor response,” *Sens. Act. B Chem.*, vol. 92, pp. 269–278, July 2003.
- [32] I. Gurin, N. Goel, and S. Bart, “Gas mixture estimation: Using power-law models of arrayed chemiresistive metal-oxide sensors,” in *2023 IEEE SENSORS*, pp. 1–4, Oct. 2023.
- [33] S. Bhattacharjee, S. Pal, P. Scheepers, and F. Dressler, “Breath patterns as signals: A machine learning-based molecular communication perspective,” in *Proc. 12th ACM Int. Conf. Nanoscale Comput. Commun.*, pp. 22–27, 2025.
- [34] M. M. Al-Zubi and M.-S. Alouini, “Macroscale molecular communication in IoT-based pipeline inspection and monitoring applications: Preliminary experiment and mathematical model,” *IEEE Open J. Commun. Soc.*, vol. 6, pp. 7541–7554, Sept. 2025.
- [35] V. Jamali, *Design and Analysis of Molecular Communication Systems*. PhD thesis, Friedrich-Alexander-Universität Erlangen-Nürnberg, 2019.
- [36] L. Bahl, J. Cocke, F. Jelinek, and J. Raviv, “Optimal decoding of linear codes for minimizing symbol error rate,” *IEEE Trans. Inf. Theory*, vol. 20, pp. 284–287, Mar. 1973.
- [37] S. Julier and J. Uhlmann, “Unscented filtering and nonlinear estimation,” *Proc. IEEE*, vol. 92, pp. 401–422, Mar. 2004.
- [38] C. Wang *et al.*, “An Effective Constellation Design for Concentration Shift Keying in Molecular Communication Systems,” *IEEE Internet Things J.*, vol. 11, pp. 10314–10324, Mar. 2024.
- [39] J. H. Friedman, J. L. Bentley, and R. A. Finkel, “An algorithm for finding best matches in logarithmic expected time,” *ACM Trans. Mathem. Softw.*, vol. 3, pp. 209–226, Sept. 1977.
- [40] P. Wang *et al.*, “Efficient nearest neighbor search using dynamic programming,” *IEEE Trans. Pattern Anal. Mach.*, vol. 48, pp. 999–1014, Jan. 2026.
- [41] Z. Hua, Y. Li, Y. Zeng, and Y. Wu, “A theoretical investigation of the power-law response of metal oxide semiconductor gas sensors i: Schottky barrier control,” *Sens. Act. B: Chem.*, vol. 255, pp. 1911–1919, Feb. 2018.